4.4.1. *Facial nerve avulsion*

Adult Fischer 344 male rats (12–14 weeks old, 200–250 g) were anesthetized with intraperitoneal injection of pentobarbital sodium (40 mg/kg). Under a dissecting microscope, the right facial nerve was exposed at its exit from the stylomastoid foramen. Using microhemostat forceps, the proximal facial nerve was avulsed by gentle traction and removed from the distal facial nerve as described previously (Sakamoto et al., 2000). Immediately following the avulsion, microsyringe was inserted into the stylomastoid foramen and 20 μl solution of AxCAhHGF (1×10^8 pfu), AxCALacZ (1×10^8 pfu) or PBS was injected through the facial canal. The wounds were covered with a small piece of gelatin sponge (Gelfoam; Pharmacia Upjohn, Bridgewater, NJ) and suture closed, and the animals were sacrificed at 1 and 4 weeks postoperation as described below.

4.4.2. *Spinal root avulsion*

Anesthetized animals were placed in a supine position. Under a dissecting microscope, the right seventh cervical segment (C7) nerve was exposed by separating the surrounding cervical muscles and connective tissue until the point where the vertebral foramen was identified. Using microhemostat forceps, the C7 ventral and dorsal roots and dorsal root ganglia (DRG) were avulsed and removed from the peripheral nerve as described previously (Watabe et al., 2000). Immediately following avulsion, a small piece of Gelfoam presoaked with 10 μl solution of AxCAhHGF (1×10^8 pfu), AxCALacZ (1×10^8 pfu) or PBS was placed in contact with the lesioned vertebral foramen. The wounds were suture closed and animals were sacrificed at 4 weeks postoperation as described below.

4.5. *HGF ELISA of brain stem tissue containing facial nucleus*

One week after facial nerve avulsion and the treatment with AxCALacZ or AxCAhHGF, the animals ($n=3$) were euthanized with a lethal dose of pentobarbital sodium and the brain stem tissue containing the facial nucleus (11–14 mg wet weight) was collected. ELISA for rat HGF and human HGF was performed as described (Sun et al., 2002; Funakoshi and Nakamura, 2003).

4.6. *Reverse transcription followed by polymerase chain reaction (RT-PCR)*

One week after facial nerve avulsion and the treatment with AxCAhHGF, the brain stem tissue containing the facial nucleus ($n=3$) was collected as described above. Total RNA was isolated from the tissue using RNA isolation reagent (TRIZOL, Invitrogen, Carlsbad, CA) according to the manufacturer's instructions and treated with RNase-free DNase (Roche, Penzberg, Germany) in transcription buffer for 30 min. First strand cDNA was synthesized from 250 ng of total RNA using random primer and Superscript II reverse transcriptase (Invitrogen) for one PCR analysis. The PCR reactions were carried out in PCR buffer containing cDNA template, 200 μM dNTPs, 2 mM $MgCl_2$, 0.2 μM of each primer and 25 unit/ml of ExTaq DNA polymerase (TaKaRa, Osaka, Japan). Specific oligonucleotide primers for PCR were designed to amplify rat HGF cDNA (Tashiro et al., 1990; GenBank Accession no. NM_017017; forward, 5′-GCCAAAACAAAA-CAACTG-3′; reverse, 5′-GACACCAAGAACCATTCTCA-3′) that yield 615 bp amplified products, and human HGF cDNA (Seki et al., 1990; M60718; forward, 5′-AAACATATCTGCGGAGGATC-3′; reverse, 5′-ACGATTTGGAATGGCACATC-3′) that give 561 bp amplified products. The PCR amplification program consisted of denaturation at 95 °C for 1 min, annealing at 55 °C for 1 min and extension at 72 °C for 1 min for 40 cycles. For negative control reactions, non-reverse transcribed RNA samples were processed for PCR to exclude the possibility of the contamination of genomic or adenoviral DNA as a source of amplified products. The PCR products were subjected to electrophoresis on a 1.5% agarose gel stained with ethidium bromide. To confirm the sequence identity of the amplified products, the PCR fragments were subcloned into pCRII (Invitrogen) and sequenced by a model 373A sequencer and the ABI PRISM BigDye Terminator Cycle Sequencing Kit (Applied Biosystems, Foster City, CA).

4.7. *Histological analysis*

Rats were anesthetized with a lethal dose of pentobarbital sodium and transcardially perfused with 0.1 M phosphate buffer, pH 7.4 (PB) followed by 4% paraformaldehyde in 0.1 M PB. The brain stem tissue containing facial nuclei and their intramedullary nerve tracts after facial nerve avulsion or the C7 spinal cord tissue after spinal root avulsion was dissected and immersion fixed in the same fixative for 2 h. As for facial nerve avulsion, we routinely checked the absence of extra-axial portion of facial nerve on the avulsed side under a dissecting microscope and confirmed the absence of any peripheral nerve tissues at the level of facial nerve outlet from the brain stem in microscopic sections prepared from every animal as described below. As for C7 spinal root avulsion, the absence of C7 ventral and dorsal roots as well as DRG on the lesioned side was confirmed under the dissecting microscope. A small longitudinal incision was made in the anterolateral white matter through the level of C7 ventral root outlets on the contralateral side in aid of identifying the level of C7 spinal ventral horn in histological sections.

For immunohistochemistry, the brain stem tissues were either embedded in paraffin or cryoprotected in 30% sucrose in 0.1 M PB and serial paraffin or cryostat sections were made. For immunostaining for HGF, deparaffinized sections were pretreated with 0.3% H_2O_2 in methanol, incubated with 0.05% trypsin for 15 min at 37 °C and preincubated with 3% heat-inactivated goat serum in 0.1% Triton-X100 in phosphate-buffered saline (T-PBS). Sections were then incubated overnight at 4 °C with rabbit anti-human HGFα antibody (H55; recognizes human and rat HGFα; IBL, Fujioka, Japan) or rat HGFα antibody (H56; recognizes rat, but not human, HGFα; IBL) diluted 1:200 in T-PBS followed by the incubation with biotinylated goat anti-rabbit IgG at a dilution of 1:200 and with ABC reagent (Vector). Immunostaining for ChAT on cryostat sections was performed using rabbit polyclonal antibody to ChAT (1:1000; Chemicon, Temecula, CA) and ABC method as described previously (Watabe et al., 2000). Sections were visualized by 3,3′-diaminobenzidine tetrahydrocholoride (DAB)–H_2O_2 solution and counterstained with hematoxylin.

For negative controls, the primary antibodies were omitted or replaced by non-immunized animal sera.

For motoneuron cell counting, serial paraffin-embedded brain stem or C7 spinal cord sections were made. Every fifth section (6 μm thickness; 24 μm interval) was picked up, deparaffinized and stained with cresyl violet (Nissl staining). Facial motoneurons having nuclei containing distinct nucleoli on both sides of the facial nuclei were counted in 25 sections. For spinal motoneuron cell counting, ventral horn motoneurons located in Rexed's lamina IX having nuclei greater than 15 μm in diameter with distinct nucleoli on both sides of the C7 spinal cord were counted in 35 sections. The data were then expressed as the mean ± SD from 4 to 8 animals, and statistical significance was assessed by Mann–Whitney U test.

Acknowledgments

We are grateful to Dr. Jing-Song Shen (Jikei University School of Medicine) for adenovirus preparation. This work was supported by Grants-in-Aid for Ministry of Education, Culture, Sports, Science and Technology, Japan, and Research on Psychiatric and Neurological Diseases and Mental Health, H16-kokoro-017, Ministry of Health, Labor and Welfare, Japan.

REFERENCES

Caton, A., Hacker, A., Naeem, A., Livet, J., Maina, F., Bladt, F., Klein, R., Birchmeier, C., Guthrie, S., 2000. The branchial arches and HGF are growth-promoting and chemoattractant for cranial motor axons. Development 127, 1751–1766.

Ebens, A., Brose, K., Leonardo, E.D., Hanson Jr., M.G., Bladt, F., Birchmeier, C., Barres, B.A., Tessier-Lavigne, M., 1996. Hepatocyte growth factor/scatter factor is an axonal chemoattractant and a neurotrophic factor for spinal motor neurons. Neuron 17, 1157–1172.

Funakoshi, H., Nakamura, T., 2003. Hepatocyte growth factor: from diagnosis to clinical applications. Clin. Chim. Acta 327, 1–23.

Hamanoue, M., Takemoto, N., Matsumoto, K., Nakamura, T., Nakajima, K., Kohsaka, S., 1996. Neurotrophic effect of hepatocyte growth factor on central nervous system neurons in vitro. J. Neurosci. Res. 43, 554–564.

Honda, S., Kagoshima, M., Wanaka, A., Tohyama, M., Matsumoto, K., Nakamura, T., 1995. Localization and functional coupling of HGF and c-Met/HGF receptor in rat brain: implication as neurotrophic factor. Brain Res. Mol. Brain Res. 32, 197–210.

Hossain, M.A., Russell, J.C., Gomez, R., Laterra, J., 2002. Neuroprotection by scatter factor/hepatocyte growth factor and FGF-1 in cerebellar granule neurons is phosphatidylinositol 3-kinase/akt-dependent and MAPK/CREB-independent. J. Neurochem. 81, 365–378.

Ikeda, K., Sakamoto, T., Marubuchi, S., Kawazoe, Y., Terashima, N., Iwasaki, Y., Kinoshita, M., Ono, S., Nakagawa, M., Watabe, K., 2003. Oral administration of a neuroprotective compound T-588 prevents motoneuron degeneration after facial nerve avulsion in adult rats. Amyotroph. Lateral. Scler. Other Mot. Neuron Disord. 4, 74–80.

Jiang, Y.M., Yamamoto, M., Kobayashi, Y., Yoshihara, T., Liang, Y., Terao, S., Takeuchi, H., Ishigaki, S., Katsuno, M., Adachi, H., Niwa, J., Tanaka, F., Doyu, M., Yoshida, M., Hashizume, Y., Sobue, G., 2005. Gene expression profile of spinal motor neurons in sporadic amyotrophic lateral sclerosis. Ann. Neurol. 57, 236–251.

Kanegae, Y., Takamori, K., Sato, Y., Lee, G., Nakai, M., Saito, I., 1996. Efficient gene activation system on mammalian cell chromosomes using recombinant adenovirus producing Cre recombinase. Gene 181, 207–212.

Kato, S., Funakoshi, H., Nakamura, T., Kato, M., Nakano, I., Hirano, A., Ohama, E., 2003. Expression of hepatocyte growth factor and c-Met in the anterior horn cells of the spinal cord in the patients with amyotrophic lateral sclerosis (ALS): immunohistochemical studies on sporadic ALS and familial ALS with superoxide dismutase 1 gene mutation. Acta Neuropathol. (Berl.) 106, 112–120.

Koliatsos, V.E., Price, W.L., Pardo, C.A., Price, D.L., 1994. Ventral root avulsion: an experimental model of death of adult motor neurons. J. Comp. Neurol. 342, 35–44.

Koyama, J., Yokouchi, K., Fukushima, N., Kawagishi, K., Higashiyama, F., Moriizumi, T., 2003. Neurotrophic effect of hepatocyte growth factor on neonatal facial motor neurons. Neurol. Res. 25, 701–707.

Maina, F., Klein, R., 1999. Hepatocyte growth factor, a versatile signal for developing neurons. Nat. Neurosci. 2, 213–217.

Miyake, S., Makimura, M., Kanegae, Y., Harada, S., Sato, Y., Takamori, K., Tokuda, C., Saito, I., 1996. Efficient generation of recombinant adenoviruses using adenovirus DNA–terminal protein complex and a cosmid bearing the full-length virus genome. Proc. Natl. Acad. Sci. U. S. A. 93, 1320–1324.

Moran, L.B., Graeber, M.B., 2004. The facial nerve axotomy model. Brain Res. Brain Res. Rev. 44, 154–178.

Naeem, A., Abbas, L., Guthrie, S., 2002. Comparison of the effects of HGF, BDNF, CT-1, CNTF, and the branchial arches on the growth of embryonic cranial motor neurons. J. Neurobiol. 51, 101–114.

Nakamura, T., Nawa, K., Ichihara, A., 1984. Partial purification and characterization of hepatocyte growth factor from serum of hepatectomized rats. Biochem. Biophys. Res. Commun. 122, 1450–1459.

Nakamura, T., Nishizawa, T., Hagiya, M., Seki, T., Shimonishi, M., Sugimura, A., Tashiro, K., Shimizu, S., 1989. Molecular cloning and expression of human hepatocyte growth factor. Nature 342, 440–443.

Novak, K.D., Prevette, D., Wang, S., Gould, T.W., Oppenheim, R.W., 2000. Hepatocyte growth factor/scatter factor is a neurotrophic survival factor for lumbar but not for other somatic motoneurons in the chick embryo. J. Neurosci. 20, 326–337.

Okura, Y., Arimoto, H., Tanuma, N., Matsumoto, K., Nakamura, T., Yamashima, T., Miyazawa, T., Matsumoto, Y., 1999. Analysis of neurotrophic effects of hepatocyte growth factor in the adult hypoglossal nerve axotomy model. Eur. J. Neurosci. 11, 4139–4144.

Ruan, R.S., Leong, S.K., Yeoh, K.H., 1995. The role of nitric oxide in facial motoneuronal death. Brain Res. 698, 163–168.

Sakamoto, T., Watabe, K., Ohashi, T., Kawazoe, Y., Oyanagi, K., Inoue, K., Eto, Y., 2000. Adenoviral vector-mediated GDNF gene transfer prevents death of adult facial motoneurons. NeuroReport 11, 1857–1860.

Sakamoto, T., Kawazoe, Y., Shen, J.S., Takeda, Y., Arakawa, Y., Ogawa, J., Oyanagi, K., Ohashi, T., Watanabe, K., Inoue, K., Eto, Y., Watabe, K., 2003a. Adenoviral gene transfer of GDNF, BDNF and TGF beta 2, but not CNTF, cardiotrophin-1 or IGF1, protects injured adult motoneurons after facial nerve avulsion. J. Neurosci. Res. 72, 54–64.

Sakamoto, T., Kawazoe, Y., Uchida, Y., Hozumi, I., Inuzuka, T., Watabe, K., 2003b. Growth inhibitory factor prevents degeneration of injured adult rat motoneurons. NeuroReport 14, 2147–2151.

Seki, T., Ihara, I., Sugimura, A., Shimonishi, M., Nishizawa, T., Asami, O., Hagiya, M., Nakamura, T., Shimizu, S., 1990. Isolation and expression of cDNA for different forms of hepatocyte growth factor from human leukocyte. Biochem. Biophys. Res. Commun. 172, 321–327.

Søreide, A.J., 1981. Variations in the axon reaction after different types of nerve lesion. Light and electron microscopic studies on the facial nucleus of the rat. Acta Anat. (Basel). 110, 173–188.

Sun, W., Funakoshi, H., Nakamura, T., 2002. Overexpression of HGF retards disease progression and prolongs life span in a transgenic mouse model of ALS. J. Neurosci. 22, 6537–6548.

Tashiro, K., Hagiya, M., Nishizawa, T., Seki, T., Shimonishi, M., Shimizu, S., Nakamura, T., 1990. Deduced primary structure of rat hepatocyte growth factor and expression of the mRNA in rat tissues. Proc. Natl. Acad. Sci. U. S. A. 87, 3200–3204.

Watabe, K., Ohashi, T., Sakamoto, T., Kawazoe, Y., Takeshima, T., Oyanagi, K., Inoue, K., Eto, Y., Kim, S.U., 2000. Rescue of lesioned adult rat spinal motoneurons by adenoviral gene transfer of glial cell line-derived neurotrophic factor. J. Neurosci. Res. 60, 511–519.

Watabe, K., Hayashi, Y., Kawazoe, Y., 2005. Peripheral nerve avulsion injuries as experimental models for adult motoneuron degeneration. Neuropathology 25, 371–380.

Wong, V., Glass, D.J., Arriaga, R., Yancopoulos, G.D., Lindsay, R.M., Conn, G., 1997. Hepatocyte growth factor promotes motor neuron survival and synergizes with ciliary neurotrophic factor. J. Biol. Chem. 272, 5187–5191.

Wu, W., 1993. Expression of nitric-oxide synthase (NOS) in injured CNS neurons as shown by NADPH diaphorase histochemistry. Exp. Neurol. 120, 153–159.

Yamamoto, Y., Livet, J., Pollock, R.A., Garces, A., Arce, V., deLapeyriere, O., Henderson, C.E., 1997. Hepatocyte growth factor (HGF/SF) is a muscle-derived survival factor for a subpopulation of embryonic motoneurons. Development 124, 2903–2913.

Zhang, L., Himi, T., Morita, I., Murota, S., 2000. Hepatocyte growth factor protects cultured rat cerebellar granule neurons from apoptosis via the phophatidylinositol-3 kinase/Akt pathway. J. Neurosci. Res. 59, 489–496.

BRAIN RESEARCH 1167 (2007) 112–117

available at www.sciencedirect.com

ScienceDirect

www.elsevier.com/locate/brainres

BRAIN RESEARCH

Research Report

Increased autophagy in transgenic mice with a *G93A* mutant *SOD1* gene

*Nobutoshi Morimoto, Makiko Nagai, Yasuyuki Ohta, Kazunori Miyazaki, Tomoko Kurata, Mizuki Morimoto, Tetsuro Murakami, Yasushi Takehisa, Yoshio Ikeda, Tatsushi Kamiya, Koji Abe**

Department of Neurology, Graduate School of Medicine, Dentistry and Pharmaceutical Sciences, Okayama University, 2-5-1 Shikata-cho, Okayama 700-8558, Japan

ARTICLE INFO

Article history:
Accepted 3 June 2007
Available online 7 July 2007

Keywords:
Autophagy
LC3
mTOR
Spinal cord
G93A
ALS

ABSTRACT

Autophagy, like the ubiquitin–proteasome system, is considered to play an important role in preventing the accumulation of abnormal proteins. Rat microtubule-associated protein 1 light chain 3 (LC3) is important for autophagy, and the conversion from LC3-I into LC3-II is accepted as a simple method for monitoring autophagy. We examined a SOD1G93A transgenic mouse model for amyotrophic lateral sclerosis (ALS) to consider a possible relationship between autophagy and ALS. In our study we analyzed LC3 and mammalian target of rapamycin (mTOR), a suppressor of autophagy, by immunoassays. The level of LC3-II, which is known to be correlated with the extent of autophagosome formation, was increased in SOD1G93A transgenic mice at symptomatic stage compared with non-transgenic or human wild-type SOD1 transgenic animals. Moreover, the ratio of phosphorylated mTOR/Ser^{2448} immunopositive motor neurons to total motor neurons was decreased in SOD1G93A-Tg mice. The present data show the possibility of increased autophagy in an animal model for ALS. And autophagy may be partially regulated by an mTOR signaling pathway in these animals.

1. Introduction

In every eukaryotic cell, there are two main systems for the degradation of cytoplasmic protein; the ubiquitin–proteasome system (Ciechanover, 2006) and autophagy (Yorimitsu and Klionsky, 2005). Macroautophagy (hereafter referred to as autophagy) is considered to be the main pathway among several subtypes of autophagy. During the process of autophagy, small cytoplasmic proteins are sequestered by autophagosomes and then degraded upon fusion with lysosomes (Baba et al., 1994). In contrast to the ubiquitin–proteasome system, which accounts for most of the selective intracellular protein degradation, autophagy is less selective (Klionsky, 2005; Levine and Klionsky, 2004). Recently, 27 autophagy-related (ATG) genes were identified whose products appear to be related to the autophagy process: these genes were characterized in yeast (Klionsky et al., 2003; Yorimitsu and Klionsky, 2005). It was found that the molecular basis of autophagy may well be highly conserved from yeast to humans (Levine and Klionsky, 2004; Reggiori and Klionsky, 2002). For example, rat microtubule-associated protein 1 light chain 3 (LC3), a mammalian homologue of Atg8 plays a critical

* *Corresponding author.* Department of Neurology, Graduate School of Medicine, Dentistry and Pharmaceutical Sciences, Okayama University, 2-5-1 Shikata-cho, Okayama 700-8558, Japan. Fax: +81 86 235 7368.
E-mail address: morinobu@cc.okayama-u.ac.jp (K. Abe).

0006-8993/$ – see front matter © 2007 Elsevier B.V. All rights reserved.
doi:10.1016/j.brainres.2007.06.045

role in the formation of autophagosomes (Kirisako et al., 1999). Recently, the study of mice deficient for autophagy-related 5 (Atg5) or autophagy-related 7 (Atg7), specifically in neurons, suggested that the continuous clearance of diffuse cytosolic proteins through basal autophagy is important to prevent the accumulation of abnormal proteins, which can disrupt neural function and ultimately lead to neurodegeneration (Hara et al., 2006; Komatsu et al., 2006; Rubinsztein, 2006).

Amyotrophic lateral sclerosis (ALS) is a neurodegenerative disease caused by a selective loss of motor neurons, with 10% of ALS cases being familial. Dominant missense mutations in the gene that encodes the Cu/Zn superoxide dismutase, *SOD1*, are responsible for 20% of familial ALS (fALS) cases. It has been well established that mutant *SOD1*-mediated toxicity is caused by a gain of toxic function rather than the loss of *SOD1* activity (Reaume et al., 1996). Kabuta and colleagues reported that autophagy reduced mutant *SOD1*-mediated toxicity and that induction of autophagy decreased mutant *SOD1* protein levels: these authors proposed that the contribution of autophagy to mutant *SOD1* degradation was comparable to that of proteasome pathway (Kabuta et al., 2006).

Although it is believed that a deficiency in autophagy causes neurodegeneration (Hara et al., 2006; Komatsu et al., 2006; Rubinsztein, 2006) and that autophagy plays a protective role against neurodegeneration (Berger et al., 2006; Iwata et al., 2005; Kabuta et al., 2006; Ravikumar et al., 2004, 2006; Webb et al., 2003), there have been no reports investigating autophagy in an *in vivo* model of ALS. Therefore, we examined autophagy in SOD1G93A transgenic mice to consider a possible relationship between autophagy and ALS.

2. Results

2.1. *Immunohistochemical analysis of LC3*

Immunohistochemical analysis showed that LC3 was expressed mainly in neurons of the spinal cords in non-transgenic mice (non-Tg) (Fig. 1A, C) and transgenic mice expressing the *G93A* mutant human *SOD1* (Tg) (Fig. 1B, D), with similar staining densities. Despite the magnification, it was difficult to detect the autophagosome. Double-labeling immunofluorescent analysis of spinal cord sections with an antibody to LC3 (Fig. 1E) and another antibody (SMI-32) against neurofilament protein (Fig. 1F) showed that LC3 existed in motor neurons in both Tg and non-Tg mice (Fig. 1G).

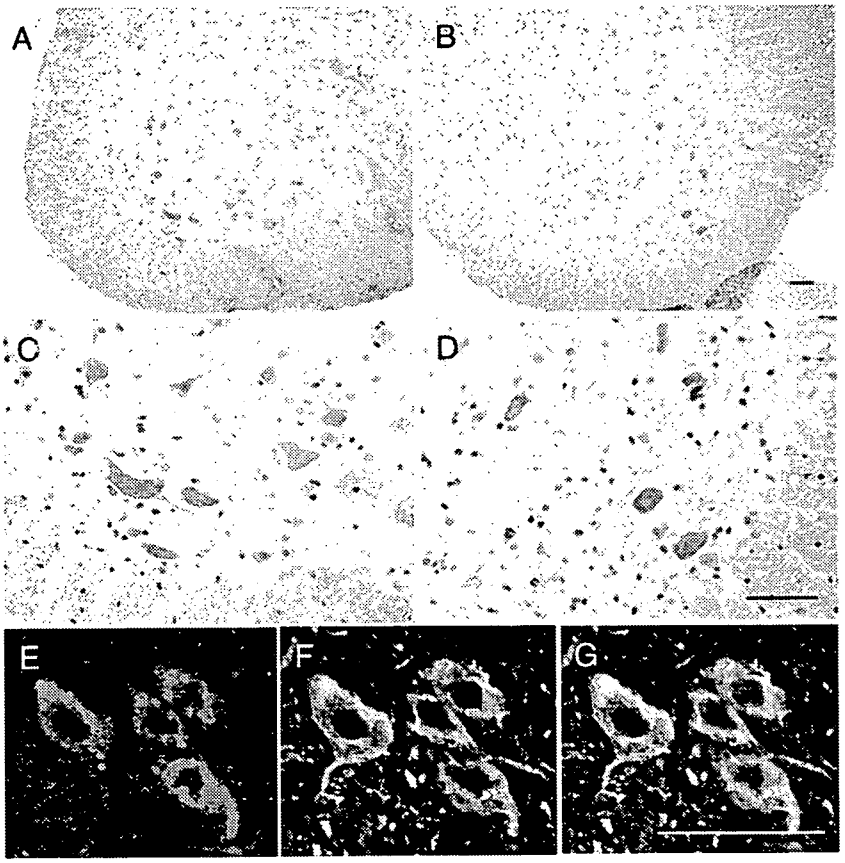

Fig. 1 – Photomicrographs of spinal cord sections from 19W SOD1G93A-Tg and non-Tg mice labeled with an antibody to LC3 and counterstained with hematoxylin–eosin. Note the LC3 expression in spinal motor neurons both of Tg mice (B, D) and non-Tg littermates (A, C). Double-labeling immunofluorescence analysis of spinal cord sections from SOD1G93A-Tg mice shows co-localization (G) of LC3 (E) and neurofilament (labeled with the monoclonal antibody SMI-32), a marker of motor neurons (F). Scale bars: 100 μm.

2.2. *Western blot analysis for LC3-II in the spinal cord*

The amount of LC3-II (relative to β-tubulin) decreased with age in non-Tg mice: 0.58±0.11 in non-Tg 10 weeks of age (W), 0.44±0.11 in non-Tg 17W, 0.32±0.06 in non-Tg 19W, mean±standard deviation (SD). Although the difference between non-Tg 10W mice and non-Tg 19W mice was highly significant; $^{**}p<0.01$, the difference between non-Tg 10W and non-Tg 17W and the difference between non-Tg 17W and non-Tg 19W were not statistically significant. Contrary to the results in non-Tg mice, the amount of LC3-II (relative to β-tubulin) in Tg mice tended to increase with age: 0.73±0.22 in Tg 10W (presymptomatic stage), 0.76±0.23 in Tg 17W (early symptomatic stage), 0.85±0.09 in Tg 19W (end symptomatic stage). However, there was no significant difference in the level of LC3-II among Tg 10W, Tg 17W and Tg 19W mice by a multiple comparison test; $p=0.61$.

The amounts of LC3-II were higher in Tg mice than in non-Tg mice at 17W: 0.44±0.11 in non-Tg vs. 0.76±0.23 in Tg; $^{*}p<0.05$, and at 19W: 0.32±0.06 in non-Tg vs. 0.85±0.09 in Tg; $^{**}p<0.01$ (Fig. 2A, B). On the other hand, at 10W, there was no significant difference between non-Tg and Tg animals: 0.58±0.11 in non-Tg vs. 0.73±0.22 in Tg; $p=0.20$.

We examined five wild-type human *SOD1* transgenic mice (WtSOD1-Tg) at 19W and confirmed that the amount of LC3-II was again higher in 19W SOD1G93A-Tg mice than in WtSOD1-Tg animals: 0.36±0.08 in WtSOD1-Tg vs. 0.85±0.09 in SOD1G93A-Tg; $^{**}p<0.01$ (Fig. 3A, B).

We also examined LC3-II in cerebellar cortex of five non-Tg 17W mice and five Tg 17W mice. There was no statistically significant difference between non-Tg and Tg mice (data not shown).

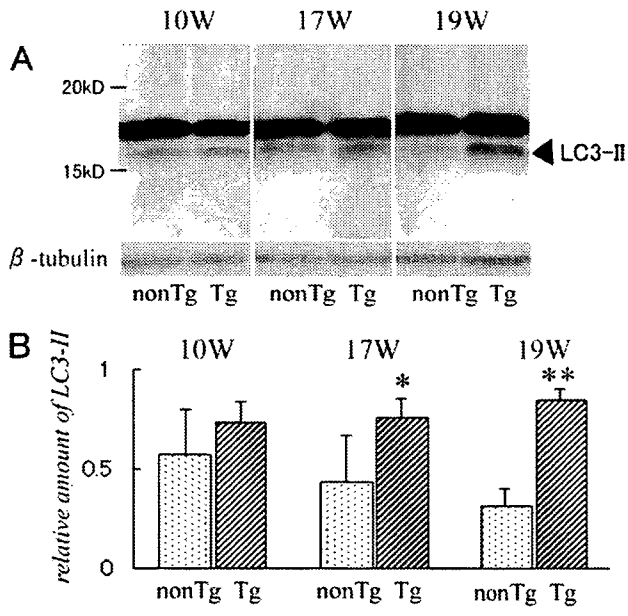

Fig. 2 – Western blot analysis of spinal cords for LC3-II protein (A) and its quantitative analysis relative to β-tubulin (B). Note the higher level of LC3-II in SOD1G93A-Tg mice than in non-Tg mice at 17W (early symptomatic stage); $n=5$, $^{*}p<0.05$ and at 19 W (end symptomatic stage); $n=5$, $^{**}p<0.01$.

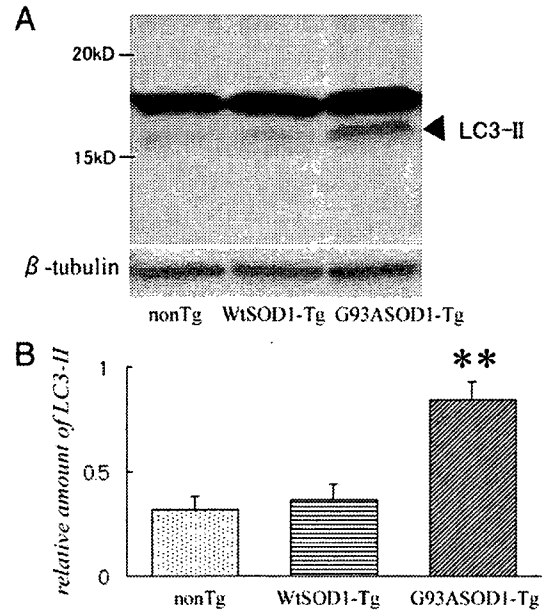

Fig. 3 – Western blot analysis of spinal cords for LC3-II protein (A) and its quantitative analysis relative to β-tubulin (B). Note the higher level of LC3-II in 19W SOD1G93A-Tg mice than in both age-matched non-Tg mice; $n=5$, $^{**}p<0.01$ and WtSOD1-Tg mice; $n=5$, $^{**}p<0.01$.

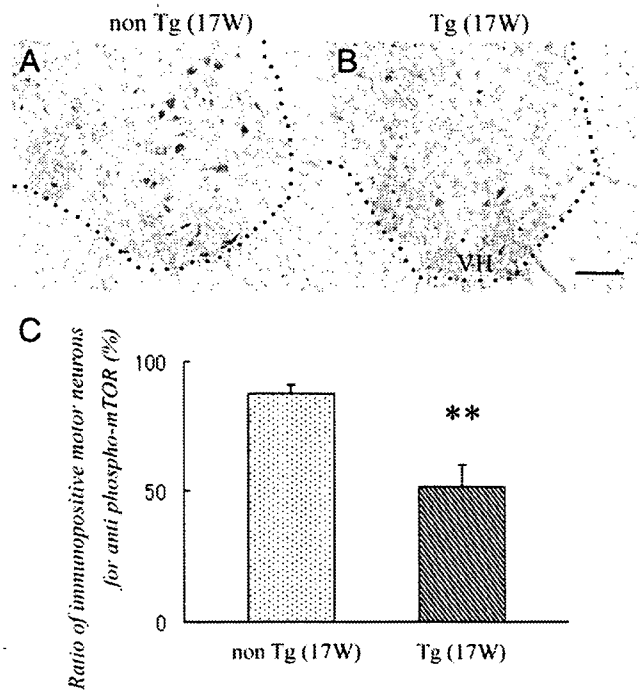

Fig. 4 – Photomicrographs of spinal cord sections labeled with antibodies to phosphorylated mTOR/Ser^{2448} (p-mTOR) (A, B). Note that the p-mTOR staining was much weaker in 17W SOD1G93A-Tg mice (B) than in age-matched non-Tg mice (A). The ratio of immunopositive motor neurons to total living motor neurons in Tg mice was significantly lower than in non-Tg mice; $n=5$, $^{**}p<0.01$, (C) at 17W. Scale bar: 100 μm. VH: ventral horn.

2.3. *Immunohistochemical analysis of phosphorylated mTOR/Ser^{2448} (p-mTOR)*

Immunohistochemical analysis of p-mTOR was performed using 17W (early symptomatic stage) mice. Immunohistochemical staining of spinal cord sections with an antibody against p-mTOR showed that the number of immunopositive motor neurons in the anterior horn areas decreased in Tg mice: 16.3±3.4/section in non-Tg vs. 4.8±0.7/section in Tg, mean±standard deviation (SD) (Fig. 4A, B). The number of living motor neurons also decreased in Tg mice: 18.6±3.7/section in non-Tg vs. 9.3±1.5/section in Tg. When the ratios of mean immunopositive motor neurons to mean living motor neurons were taken with each five Tg and five non-Tg mice, the average ratio of Tg mice was significantly lower than that of non-Tg mice: 87.6±3.6% in non-Tg vs. 52.1±8.1% in Tg; $^{**}p<0.01$ (Fig. 4C).

3. Discussion

LC3 is associated with autophagosome membranes after post-translational modifications. A C-terminal fragment of LC3 is cleaved immediately after synthesis to yield a cytosolic form called LC3-I (18 kDa). A subpopulation of LC3-I is further converted to an autophagosome-associating form, LC3-II (16 kDa). Kabeya et al. reported that the amount of LC3-II was correlated with the extent of autophagosome formation (Kabeya et al., 2000, 2004). The conversion of LC3-I into LC3-II is accepted as a simple method for monitoring autophagy (Mizushima, 2004). Consequently, we measured the extent of autophagy in fALS model mice by determination of LC3-II expression with immunoassays. Although there are more direct methods for monitoring autophagy, for example, the green fluorescent protein (GFP)-LC3 transgenic mouse (Mizushima et al., 2004) or electron microscopic analysis, our present study focused on the amount of LC3-II for simplicity. Our immunohistochemical data showed that LC3 was expressed mainly in neurons of the spinal cords both in non-Tg and Tg mice (Fig. 1). Thus, it may be considered that Western blot analysis using the whole tissue from ventral portion of the lumbar spinal cord demonstrates the extent of autophagy mainly in motor neurons that were affected by the disease.

In our study, the amount of LC3-II decreased with age in non-Tg mice (Fig. 2), consistent with reports that autophagic activity declines with age from experiments in rat (Del Roso et al., 2003). By contrast, the level of LC3-II tended to increase with age in SOD1G93A-Tg mice, and was significantly higher when compared with non-Tg littermates or WtSOD1-Tg animals (Figs. 2 and 3), suggesting that autophagosome formation increased in SOD1G93A-Tg mice. The present data show the possibility of increased autophagy in an animal model for ALS.

However, there are two ways to explain increased autophagosome formation; that autophagy is upregulated to clear the mutant proteins or that delaying the clearance of autophagosomes causes increased autophagosome formation. To confirm which hypothesis is true, assay of the lysosomal enzyme or measuring the clearance time of autophagosomes is needed.

Several genes/proteins that regulate mammalian autophagy have recently been identified. Mammalian target of rapamycin (mTOR) is a phosphatidyl inositol kinase-related kinase that negatively regulates autophagy (Schmelzle and Hall, 2000; Yorimitsu and Klionsky, 2005). It has been reported that mTOR function is activated by phosphorylation of Ser^{2448} (Nave et al., 1999; Ravikumar et al., 2003). In our study, we confirmed that the level of phosphorylated mTOR/Ser^{2448}, an activated form, decreased in SOD1G93A mutants at early symptomatic stage (Fig. 4); therefore, it is possible that autophagy is partially regulated by the mTOR intracellular signaling pathway.

There is a hypothesis that inclusion inactivates mTOR by sequestration and induces autophagy. Ravikumar and colleagues showed that mTOR was sequestered into polyglutamine-containing aggregates in cell models, transgenic mice and the brains of patients with Huntington disease. Sequestration of mTOR impairs its kinase activity and induces autophagy, a key clearance pathway for mutant huntingtin fragments. Then, induced autophagy protects against polyglutamine toxicity, as the specific mTOR inhibitor rapamycin attenuates huntingtin accumulation and cell death in cell models of Huntington disease, whereas inhibition of autophagy has the converse effect (Ravikumar et al., 2004). We considered that the appearance of mutant SOD1 aggregates in motor neurons in fALS patients and mouse models (Bruijn et al., 1997; Kato et al., 2000; Watanabe et al., 2001) suggested the existence of a similar protective pathway in fALS animals and patients.

On the other hand, recent studies have presented the evidence that insulin signal stimulates phosphorylation and activity of mTOR via Akt/PKB (Schmelzle and Hall, 2000). And Nagano et al. reported that the expressions of PI3-K and Akt/PKB were decreased in SOD1G93A-Tg mice (Nagano et al., 2002). It can also be hypothesized that the reduction of mTOR phosphorylation may be mediated by reduced PI3-K and Akt/PKB signaling in these transgenic animals.

Further research is necessary to elucidate the mechanisms of regulation for autophagy and the role of autophagy toward the motor neuron death in SOD1G93A-Tg mice.

4. Experimental procedures

4.1. *Animal model*

All experimental procedures were carried out according to the guidelines of the Animal Care and Use Committee of the Graduate School of Medicine and Dentistry of Okayama University. Transgenic mice expressing the G93A mutant human *SOD1* (strain B6SJL-TGN (SOD1G93A) 1GUR^{dl}) or wild-type human *SOD1* (strain C57BL/6J-TGN (SOD1) 2GUR^{dl}) were originally obtained from the Jackson Laboratory (Bar Harbor, ME; Gurney et al., 1994), then backcrossed onto a C57BL/6 background strain by mating hemizygote males with inbred C57BL/6 female mice (C57BL/6CrSlc, Nihon SLC, Sizuoka, Japan) to produce transgenic (Tg) and non-transgenic littermates (non-Tg). Our SOD1G93A-Tg mice experienced disease onset at about 15W and died at approximately 20W. In our

study, there were three experimental groups: 10W, 17W and 19W. Each group contained five Tg mice and five age-matched non-Tg mice ($n=5$).

4.2. *Primary antibodies*

The anti-LC3 antibody was obtained from Medical Biological Laboratories (#PD012). The anti-phosphorylated mTOR/Ser^{2448} antibody was obtained from Cell Signaling Technologies, and SMI-32, a marker of motor neurons, was from Berkeley Antibody Company.

4.3. *Histological analysis*

Animals were deeply anesthetized and transcardially perfused with heparinized saline, followed by 4% paraformaldehyde in 0.1 M phosphate buffer (pH 7.4). The region of the spinal cord spanning L4–5 was removed and further fixed by immersion in the same fixative for 4 h, then frozen after cryoprotection with a series of phosphate-buffered sucrose solutions of increasing concentration (10%, 15% and 20%). Transverse sections of 10 μm thickness were cut through the middle of the L4 segment on a cryostat. The LC3 antibody was used at a dilution of 1:250, and the antibody against phosphorylated mTOR/Ser^{2448} was used at 1:100. Five transverse sections from each lumbar cord were used for all histological analysis. We carried out immunohistochemical analysis by standard fluorescence methods or peroxidase labeling using the Vectastain Avidin:Biotinylated enzyme Complex (ABC) kit. We analyzed relevant negative controls without primary antibodies alongside all experiments.

4.4. *Motor neuron count*

For evaluating the percentage of immunopositive motor neurons, preserved motor neurons in the L4 segment were counted in five transverse sections from each lumbar cord stained with cresyl violet (Nissl stain). All cells in ventral horns below a lateral line across the spinal cord from the central canal were microscopically video-captured, and only cells with a diameter greater than 20 μm that showed clear nucleoli were counted by investigators who were blinded to the sample information, as described previously (Ohta et al., 2006). The average of five sections was taken as the number of living motor neurons of each animal. In addition, each mouse section was immunostained for anti-choline acetyltransferase antibody (ChAT goat antiserum; Chemicon, Temecula, CA) to confirm the results of motor neuron counting.

4.5. *Western blot analysis*

Western blot analysis was performed using the ventral portion of the lumbar spinal cord of five mice from each group. We added 0.3 mL of cold lysis buffer (50 mM Tris–HCl, pH 7.2, 10% glycerol, 250 mM NaCl, 0.1% NP-40, 2 mM EDTA and protease inhibitors) to the spinal cord tissue and homogenized it at 4 °C. The homogenate was centrifuged at 12,000 rpm at 4 °C, and the supernatant was used for Western blotting. We carried out Western blot analysis using standard techniques with an ECL Plus detection kit (GE Healthcare). The dilution of the anti-LC3 antibody was 1:500. We carried out densitometry analysis using Scion Image Beta 4.02 software and took the average of the five mice. Data obtained were analyzed by Student's t-test.

Acknowledgments

This work was partially supported by Grants-in-Aid for Scientific Research (B) 15390273 and (Hoga) 15659338 and the National Project on Protein Structural and Functional Analyses from the Ministry of Education, Science, Culture and Sports of Japan and by grants from the Ministry of Health and Welfare of Japan (to Y. Itoyama, I. Kimura, and S. Kuzuhara).

REFERENCES

Baba, M., Takeshige, K., Baba, N., Ohsumi, Y., 1994. Ultrastructural analysis of the autophagic process in yeast: detection of autophagosomes and their characterization. J. Cell Biol. 124, 903–913.

Berger, Z., Ravikumar, B., Menzies, F.M., Oroz, L.G., Underwood, B.R., Pangalos, M.N., Schmitt, I., Wullner, U., Evert, B.O., O'Kane, C.J., Rubinsztein, D.C., 2006. Rapamycin alleviates toxicity of different aggregate-prone proteins. Hum. Mol. Genet. 15, 433–442.

Bruijn, L.I., Becher, M.W., Lee, M.K., Anderson, K.L., Jenkins, N.A., Copeland, N.G., Sisodia, S.S., Rothstein, J.D., Borchelt, D.R., Price, D.L., Cleveland, D.W., 1997. ALS-linked *SOD1* mutant G85R mediates damage to astrocytes and promotes rapidly progressive disease with *SOD1*-containing inclusions. Neuron 18, 327–338.

Ciechanover, A., 2006. The ubiquitin proteolytic system: from a vague idea, through basic mechanisms, and onto human diseases and drug targeting. Neurology 66, S7–S19.

Del Roso, A., Vittorini, S., Cavallini, G., Donati, A., Gori, Z., Masini, M., Pollera, M., Bergamini, E., 2003. Ageing-related changes in the in vivo function of rat liver macroautophagy and proteolysis. Exp. Gerontol. 38, 519–527.

Gurney, M.E., Pu, H., Chiu, A.Y., Dal Canto, M.C., Polchow, C.Y., Alexander, D.D., Caliendo, J., Hentati, A., Kwon, Y.W., Deng, H.X., et al., 1994. Motor neuron degeneration in mice that express a human Cu,Zn superoxide dismutase mutation. Science 264, 1772–1775.

Hara, T., Nakamura, K., Matsui, M., Yamamoto, A., Nakahara, Y., Suzuki-Migishima, R., Yokoyama, M., Mishima, K., Saito, I., Okano, H., Mizushima, N., 2006. Suppression of basal autophagy in neural cells causes neurodegenerative disease in mice. Nature 441, 885–889.

Iwata, A., Christianson, J.C., Bucci, M., Ellerby, L.M., Nukina, N., Forno, L.S., Kopito, R.R., 2005. Increased susceptibility of cytoplasmic over nuclear polyglutamine aggregates to autophagic degradation. Proc. Natl. Acad. Sci. U. S. A. 102, 13135–13140.

Kabeya, Y., Mizushima, N., Ueno, T., Yamamoto, A., Kirisako, T., Noda, T., Kominami, E., Ohsumi, Y., Yoshimori, T., 2000. LC3, a mammalian homologue of yeast Apg8p, is localized in autophagosome membranes after processing. Embo J. 19, 5720–5728.

Kabeya, Y., Mizushima, N., Yamamoto, A., Oshitani-Okamoto, S., Ohsumi, Y., Yoshimori, T., 2004. LC3, GABARAP and GATE16 localize to autophagosomal membrane depending on form-II formation. J. Cell Sci. 117, 2805–2812.

Kabuta, T., Suzuki, Y., Wada, K., 2006. Degradation of amyotrophic lateral sclerosis-linked mutant Cu,Zn-superoxide dismutase proteins by macroautophagy and the proteasome. J. Biol. Chem. 281, 30524–30533.

Kato, S., Takikawa, M., Nakashima, K., Hirano, A., Cleveland, D.W., Kusaka, H., Shibata, N., Kato, M., Nakano, I., Ohama, E., 2000. New consensus research on neuropathological aspects of familial amyotrophic lateral sclerosis with superoxide dismutase 1 (SOD1) gene mutations: inclusions containing SOD1 in neurons and astrocytes. Amyotroph. Lateral Scler. Other Mot. Neuron Disord. 1, 163–184.

Kirisako, T., Baba, M., Ishihara, N., Miyazawa, K., Ohsumi, M., Yoshimori, T., Noda, T., Ohsumi, Y., 1999. Formation process of autophagosome is traced with Apg8/Aut7p in yeast. J. Cell Biol. 147, 435–446.

Klionsky, D.J., 2005. The molecular machinery of autophagy: unanswered questions. J. Cell Sci. 118, 7–18.

Klionsky, D.J., Cregg, J.M., Dunn Jr., W.A., Emr, S.D., Sakai, Y., Sandoval, I.V., Sibirny, A., Subramani, S., Thumm, M., Veenhuis, M., Ohsumi, Y., 2003. A unified nomenclature for yeast autophagy-related genes. Dev. Cell 5, 539–545.

Komatsu, M., Waguri, S., Chiba, T., Murata, S., Iwata, J., Tanida, I., Ueno, T., Koike, M., Uchiyama, Y., Kominami, E., Tanaka, K., 2006. Loss of autophagy in the central nervous system causes neurodegeneration in mice. Nature 441, 880–884.

Levine, B., Klionsky, D.J., 2004. Development by self-digestion: molecular mechanisms and biological functions of autophagy. Dev. Cell 6, 463–477.

Mizushima, N., 2004. Methods for monitoring autophagy. Int. J. Biochem. Cell Biol. 36, 2491–2502.

Mizushima, N., Yamamoto, A., Matsui, M., Yoshimori, T., Ohsumi, Y., 2004. In vivo analysis of autophagy in response to nutrient starvation using transgenic mice expressing a fluorescent autophagosome marker. Mol. Biol. Cell 15, 1101–1111.

Nagano, I., Murakami, T., Manabe, Y., Abe, K., 2002. Early decrease of survival factors and DNA repair enzyme in spinal motor neurons of presymptomatic transgenic mice that express a mutant SOD1 gene. Life Sci. 72, 541–548.

Nave, B.T., Ouwens, M., Withers, D.J., Alessi, D.R., Shepherd, P.R., 1999. Mammalian target of rapamycin is a direct target for protein kinase B: identification of a convergence point for opposing effects of insulin and amino-acid deficiency on protein translation. Biochem. J. 344 (Pt 2), 427–431.

Ohta, Y., Nagai, M., Nagata, T., Murakami, T., Nagano, I., Narai, H., Kurata, T., Shiote, M., Shoji, M., Abe, K., 2006. Intrathecal injection of epidermal growth factor and fibroblast growth factor 2 promotes proliferation of neural precursor cells in the spinal cords of mice with mutant human SOD1 gene. J. Neurosci. Res. 84, 980–992.

Ravikumar, B., Stewart, A., Kita, H., Kato, K., Duden, R., Rubinsztein, D.C., 2003. Raised intracellular glucose concentrations reduce aggregation and cell death caused by mutant huntingtin exon 1 by decreasing mTOR phosphorylation and inducing autophagy. Hum. Mol. Genet. 12, 985–994.

Ravikumar, B., Vacher, C., Berger, Z., Davies, J.E., Luo, S., Oroz, L.G., Scaravilli, F., Easton, D.F., Duden, R., O'Kane, C.J., Rubinsztein, D.C., 2004. Inhibition of mTOR induces autophagy and reduces toxicity of polyglutamine expansions in fly and mouse models of Huntington disease. Nat. Genet. 36, 585–595.

Ravikumar, B., Berger, Z., Vacher, C., O'Kane, C.J., Rubinsztein, D.C., 2006. Rapamycin pre-treatment protects against apoptosis. Hum. Mol. Genet. 15, 1209–1216.

Reaume, A.G., Elliott, J.L., Hoffman, E.K., Kowall, N.W., Ferrante, R.J., Siwek, D.F., Wilcox, H.M., Flood, D.G., Beal, M.F., Brown Jr., R.H., Scott, R.W., Snider, W.D., 1996. Motor neurons in Cu/Zn superoxide dismutase-deficient mice develop normally but exhibit enhanced cell death after axonal injury. Nat. Genet. 13, 43–47.

Reggiori, F., Klionsky, D.J., 2002. Autophagy in the eukaryotic cell. Eukaryot. Cell 1, 11–21.

Rubinsztein, D.C., 2006. The roles of intracellular protein-degradation pathways in neurodegeneration. Nature 443, 780–786.

Schmelzle, T., Hall, M.N., 2000. TOR, a central controller of cell growth. Cell 103, 253–262.

Watanabe, M., Dykes-Hoberg, M., Culotta, V.C., Price, D.L., Wong, P.C., Rothstein, J.D., 2001. Histological evidence of protein aggregation in mutant SOD1 transgenic mice and in amyotrophic lateral sclerosis neural tissues. Neurobiol. Dis. 8, 933–941.

Webb, J.L., Ravikumar, B., Atkins, J., Skepper, J.N., Rubinsztein, D.C., 2003. Alpha-Synuclein is degraded by both autophagy and the proteasome. J. Biol. Chem. 278, 25009–25013.

Yorimitsu, T., Klionsky, D.J., 2005. Autophagy: molecular machinery for self-eating. Cell Death Differ. 12 (Suppl 2), 1542–1552.

Journal of Neuroscience Research 84:980–992 (2006)

Intrathecal Injection of Epidermal Growth Factor and Fibroblast Growth Factor 2 Promotes Proliferation of Neural Precursor Cells in the Spinal Cords of Mice With Mutant Human SOD1 Gene

Yasuyuki Ohta, Makiko Nagai, Tetsuya Nagata, Tetsuro Murakami, Isao Nagano, Hisashi Narai, Tomoko Kurata, Mito Shiote, Mikio Shoji, and Koji Abe*

Department of Neurology, Graduate School of Medicine, Dentistry and Pharmacy, Okayama University, Okayama, Japan

We investigated three steps of neural precursor cell activation—proliferation, migration, and differentiation—in amyotrophic lateral sclerosis spinal cord treated with intrathecal infusion of epidermal growth factor (EGF) and fibroblast growth factor 2 (FGF2) into the lumbar spinal cord region of normal and symptomatic transgenic (Tg) mice with a mutant human Cu/Zn superoxide dismutase (SOD1) gene. We observed that 5-bromodeoxyuridine (BrdU) + nestin double-labeled neural precursor cells increased in the spinal cords of Tg mice compared with non-Tg mice, with a much greater increase produced by EGF and FGF2 treatment. The number of BrdU + nestin double-labeled cells was larger than that of BrdU + ionized calcium-binding adapter molecule-1 (Iba1), BrdU + glial fibrillary acidic protein (GFAP), or BrdU + highly polysialylated neural cell adhesion molecule (PSA-NCAM) double-labeled cells, but none expressed neuronal nuclear antigen (NeuN). On further analysis of the gray matter of Tg mice, the number of BrdU + nestin and BrdU + PSA-NCAM double-labeled cells increased more in the ventral horns than the dorsal horns, which was again greatly enhanced by EGF and FGF2 treatment. Because neural precursor cells reside close to the ependyma of central canal, the present study suggests that proliferation and migration of neural precursor cells to the ventral horns is greatly activated in symptomatic Tg mice and is further enhanced by EGF and FGF2 treatment and, furthermore, that the neural precursor cells preferentially differentiate into neuronal precursor cells instead of astrocytes in Tg mice with EGF and FGF2 treatment.

Key words: neural precursor cells; epidermal growth factor; fibroblast growth factor 2; spinal cord; amyotrophic lateral sclerosis

Amyotrophic lateral sclerosis (ALS) is a progressive, fatal neurodegenerative disease that is characterized by selective loss of central and peripheral motor neurons. There are many hypotheses about the cause of this disease, for example, glutamate toxicity (Bruijn et al., 2004; Ganel et al., 2006), axonal transport deficiency (Farah et al., 2003; Rao and Nixon, 2003; Kieran et al., 2005), lack of trophic factor (Murakami et al., 2003; Bruijn et al., 2004; Narai et al., 2005), and mitochondrial dysfunction (Menzies et al., 2002; Kirkinezos et al., 2005; Manfredi and Xu, 2005). In approximately 15–20% of familial ALS cases, a variety of dominant missense mutations or small deletions in the Cu/Zn superoxide dismutase (SOD1) gene has been identified (Deng et al., 1993; Rosen et al., 1993; Brown and Robberecht, 2001). Several lines of transgenic (Tg) mice have been established that express a mutant human SOD1 gene and thus act as valuable models of human ALS (Gurney et al., 1994; Wong et al., 1995). These Tg mice have proved to be the best model to date for ALS studies.

Recent studies have shown that the adult brain has the ability to produce new neurons (Doetsch et al., 1997; Alvarez-Buylla and Garcia-Verdugo, 2002; Nakatomi et al., 2002). There are endogenous neural precursor cells in the subventricular zone and subgranular zone of the dentate gyrus. Division of these cells is enhanced by traumatic and ischemic brain injury, and differentiation of these cells into neurons is activated (Yagita et al., 2001; Iwai et al., 2002, 2003; Nakatomi et al., 2002;

Contract grant sponsor: National Project on Protein Structural and Functional Analyses from the Ministry of Education, Science, Culture and Sports of Japan; Contract grant number: 15390273; Contract grant number: 15659338; Contract grant sponsor: Ministry of Health and Welfare of Japan.

*Correspondence to: Prof. Koji Abe, Department of Neurology, Graduate School of Medicine, Dentistry and Pharmacy, Okayama University, 2-5-1 Shikata-cho, Okayama 700-8558, Japan.
E-mail: yasuyuki@cc.okayama-u.ac.jp

Received 15 March 2006; Revised 5 June 2006; Accepted 19 June 2006

Published online 10 August 2006 in Wiley InterScience (www.interscience.wiley.com). DOI: 10.1002/jnr.21017

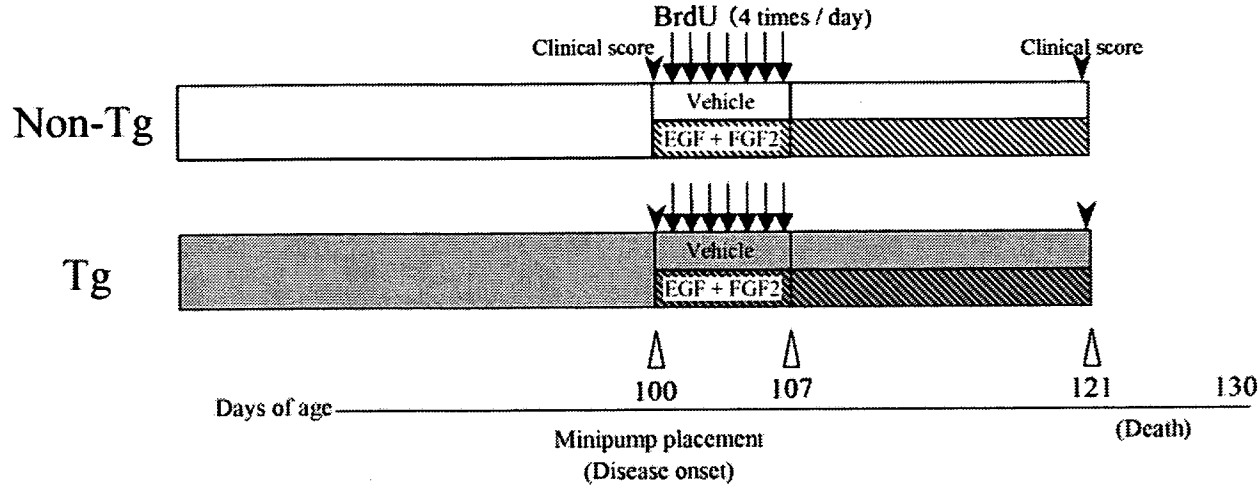

Fig. 1. Experimental paradigm for EGF and FGF2 treatment, BrdU injection, and sacrifice of mice. EGF and FGF2 or vehicle was first intrathecally infused in both non-Tg and Tg mice using osmotic minipumps at 100 days of age (average disease onset day) and lasting for 7 days. After minipump placement, clinical scores for all the mice were evaluated for the first time. BrdU was intraperitoneally injected four times per day for these 7 days in all groups. At 21 days after minipump placement, clinical scores were evaluated for the second time, and the mice were sacrificed.

Rice et al., 2003; Jin et al., 2003). In normal spinal cord, endogenous neural precursor cells reside close to the ependyma of the central canal (CC; Johansson et al., 1999; Martens et al., 2002), and these differentiate mainly into glial cells (Horner et al., 2000). In injured spinal cord, neural and glial precursor cells are activated to proliferate (Kojima and Tator, 2002; Lang et al., 2004; Mothe and Tator, 2005; Zai and Wrathall, 2005). However, most of these neural precursor cells differentiate into glial cells, and rarely into neurons. Proliferation of neural precursor cells in ALS spinal cord has not been reported in detail.

Epidermal growth factor (EGF) and fibroblast growth factor 2 (FGF2) have both neuroprotective and cell proliferative effects, but the combination of EGF and FGF2 has much stronger cell proliferative effects than either EGF or FGF2 alone in normal and injured brain and spinal cord (Alonso, 1999; Kojima and Tator, 2002; Martens et al., 2002; Nakatomi et al., 2002). However, a comprehensive study of stem cell activation in ALS spinal cord using EGF and FGF2 has not been reported. In the present study, therefore, we intrathecally infused EGF and FGF2 into the lumbar spinal cord region of normal mice and symptomatic Tg mice with a mutant human SOD1 gene and examined the proliferation, migration, and differentiation of intrinsic neural precursor cells in the lumbar spinal cord.

MATERIALS AND METHODS

Animal Model

All experimental procedures were carried out according to the guidelines of the Animal Care and Use Committee of the Graduate School of Medicine and Dentistry of Okayama University. A Tg mouse line with the G93A human SOD1 mutation (G1H/+) was obtained from Jackson Laboratories (Bar Harbor, ME; Gurney et al., 1994). G93A Tg mice experience disease onset at about 100 days of age and die approximately 20–30 days later. One-hundred-day-old G93A Tg male mice (Tg) and age-matched non-Tg wild-type B6SJL male littermates (non-Tg) were examined simultaneously. There were four experimental groups: non-Tg mice treated with vehicle (n = 6), non-Tg mice treated with recombinant human EGF (catalog No. 1376454; Roche Pharmaceutical, Tokyo, Japan) and recombinant human FGF2 (catalog No. 1120417; Roche; n = 6), Tg mice treated with vehicle (n = 8), and Tg mice treated with EGF and FGF2 (n = 8).

EGF and FGF2 Infusion

EGF and FGF2 were dissolved in phosphate-buffered saline (PBS) at a concentration of 20 μg/ml. For continuous intrathecal infusion into the lumbar spinal cord region of each animal at 100 days of age, the solution was loaded into an osmotic minipump (Alzet minipump, model 2001; Alza Corporation, Palo Alto, CA), which was designed for a nominal infusion rate of 1 μl/hr for 7 days and was attached to sterile polyethylene tubing (Becton Dickinson, Sparks, MD). Under anesthesia achieved by an intraperitoneal injection of ketamine hydrochloride (50 mg/kg; Sankyo Pharmaceuticals, Tokyo, Japan) and xylazine (12 mg/kg; Bayer AG, Leverkusen, Germany), the minipump was placed subcutaneousuly at a lumbar site. A rostrally directed cannula was threaded through the muscle close to the exposed region of the spinal column, and the tip of the cannula was placed in the spinal subarachnoid space at the level of L6 to S1. Infusion of EGF and FGF2 or vehicle (PBS) was continued for 7 days (Fig. 1).

5-Bromodeoxyuridine Labeling

A cell proliferation marker, 5-bromodeoxyuridine (BrdU; Sigma, St. Louis, MO), was dissolved in saline. After placement

of the minipump, intraperitoneal injections of BrdU began. Injections contained a dose of 50 mg/kg BrdU and were given every 6 hr (four times per day) for 7 days (total of 28 injections). By using this method, we were able to label all the cells that initiated DNA synthesis during days 1–7 (Fig. 1).

Clinical Scores

The clinical scores of the mice were evaluated twice: once following minipump placement and once 21 days after minipump placement (Fig. 1). Body weight was measured, and a rotarod test was administered to assess behavior. Based on our previous rotarod testing method (Abe et al., 1997; Klivenyi et al., 1999; Manabe et al., 2002), initially mice were placed on a rod that was rotated at 1 rpm. The speed was then increased by 1 rpm every 10 sec until the mouse fell off. The number of rotations before the mouse fell off was recorded as an indicator of each mouse's grasping power.

Motor Neuron Count

After the second clinical score evaluation, animals were deeply anesthetized with an intraperitoneal infusion of sodium pentobarbital (10 mg; Abbott Laboratories, Abbott Park, IL) and transcardially perfused with heparinized saline, followed by 4% paraformaldehyde in 0.1 M phosphate buffer (pH 7.4). The region of the spinal cord spanning L4–L5 was removed and further fixed by immersion in the same fixative for 4 hr, then frozen after cryoprotection with a series of phosphate-buffered sucrose solutions of increasing concentration (10%, 15%, and 20%).

Transverse sections of 10 μm thickness were cut through the middle of the L4 segment with a cryostat, and the motor neurons in L4 were counted in five transverse sections from each lumbar cord after staining with cresyl violet (Nissl stain). All cells in both ventral horns (VH) below a lateral line across the spinal cord from the central canal were microscopically video-captured, and only cells with a diameter greater than 20 μm that showed clear nucleoli were counted by investigators, who were blinded to the treatment conditions. In addition, five sections from each mouse were immunostained for choline acetyltransferase (ChAT goat antiserum; Chemicon, Temecula, CA) using a Vector ABC kit (Vector Laboratories, Burlingame, CA) to confirm the results of the motor neuron counting in the Nissl-stained sections.

Immunofluorescence Analysis

To determine whether the BrdU-labeled cells are neural or neuronal precursor cells, or are microglial cells, or differentiate into neuronal or astroglial cells, we performed double-immunofluorescence studies using BrdU plus nestin, highly polysialylated neural cell adhesion molecule (PSA-NCAM), ionized calcium-binding adapter molecule-1 (Iba1), neuronal nuclear antigen (NeuN), or glial fibrillary acidic protein (GFAP). To undertake detailed analysis for the BrdU + nestin and BrdU + GFAP double-labeled cells, we performed triple-immunofluorescence studies with BrdU, nestin, and GFAP. Nestin, PSA-NCAM, Iba1, NeuN, and GFAP are markers of neural precursor, neuronal precursor, microglial, differentiating neuronal, and astroglial cells, respectively.

The sections were first incubated in 2 N HCl at 25°C for 20 min to denature the DNA, then rinsed in 0.1 M boric acid (pH 8.5) at 25°C for 10 min. The sections were next incubated with rat monoclonal anti-BrdU (1:100; Oxford Biotechnology, Oxfordshire, United Kingdom) and antibody for each cellular marker, that is, mouse monoclonal anti-nestin (1:100; Chemicon), mouse monoclonal anti-PSA-NCAM (1:200; Chemicon), rabbit polyclonal anti-Iba1 (1:200; Wako, Osaka, Japan), mouse monoclonal anti-NeuN (1:400; Chemicon), or goat polyclonal anti-GFAP (1:100; Santa Cruz Biotechnology, Santa Cruz, CA) for double-immunofluorescence studies or rabbit polyclonal anti-GFAP (1:1,000; Dako, Copenhagen, Denmark) for triple-immunofluorescence studies overnight at 4°C. After being washed in PBS, the sections were incubated simultaneously with fluorescein isothiocyanate-labeled donkey anti-rat IgG (1:100; Chemicon) and Texas red-labeled horse anti-mouse IgG (1:100; Vector Laboratories), tetramethylrhodamine isothyocyanate (TRITC)-labeled goat anti-rabbit IgG (1:100; Vector Laboratories), TRITC-labeled rabbit anti-goat IgG (1:100; Vector Laboratories), or Alexa Fluor 405-labeled goat anti-rabbit IgG (1:100; Molecular Probes, Invitrogen, Eugene, OR) for 1 hr at room temperature. To confirm the specificity of the primary antibody, a set of sections was stained in a similar way without the anti-BrdU, anti-nestin, anti-PSA-NCAM, anti-Iba1, anti-NeuN, or anti-GFAP antibodies.

The sections for double-immunofluorescence studies were scanned by using a confocal microscope equipped with an argon and HeNe1 laser (LSM-510; Zeiss, Jena, Germany), and those for triple-immunofluorescence studies were scanned using a confocal microscope equipped with LD405, argon, and HeNe1 laser (FV300; Olympus, Tokyo, Japan). Sets of fluorescent images for double-immunofluorescence studies were acquired sequentially for the green and red channels to prevent crossover of signals from the green to the red or from the red to the green channels, and those for triple-immunofluorescence studies were acquired in the same manner. For quantification of the number of BrdU-labeled cells, the positively stained cells were counted in 1,024 pixels from a 450-μm × 450-μm area from five transverse sections of each lumbar cord per animal. We noted the total number and the regional differences among the gray matter (GM), white matter (WM), and CC and carried out closer analysis of the GM between the VH and both dorsal horns (DH), which are above a lateral line across the spinal cord from the central canal. In the same manner, the double-labeled cells were also counted for BrdU + nestin, BrdU + PSA-NCAM, BrdU + Iba1, BrdU + NeuN, and BrdU + GFAP.

Statistical Analysis

Results are expressed as mean ± SD. Statistical differences between groups with respect to body weight and rotarod test score were evaluated by using Welch's *t*-test. Differences between groups in the motor neuron count were evaluated by using Student's *t*-test. For the immunofluorescence studies, the cell count in each class was evaluated by using Mann-

TABLE I. Clinical Score at 121 Days of Age†

	Non-Tg		Tg	
	Vehicle	EGF + FGF2	Vehicle	EGF + FGF2
Body weight (g)	22.5 ± 2.8	20.3 ± 1.5	22.5 ± 1.9	23.1 ± 1.6
Rotarod score (rotation number)	371.6 ± 155.1	437.4 ± 104.9	63.3 ± 53.8*	62.4 ± 77.4**

†EGF and FGF2 or vehicle were intrathecally infused into lumber spinal cord region of non-Tg and Tg mice at 100 days of age using osmotic minipumps for 7 days. Clinical scores of the mice were evaluated at 121 days of age (21 days after minipump placement). Data are presented as mean ± SD of body weight (g) and rotation number in rotarod test.

*$P < 0.01$ compared with non-Tg mice with vehicle.

**$P < 0.01$ compared with non-Tg mice with EGF and FGF2.

Whitney's U test. Statistical significance was accepted at $P < 0.05$.

RESULTS

Clinical Scores

After minipump placement, no significant differences were observed in either body weight or rotarod score between non-Tg and Tg mice or those with or without EGF and FGF2 (data not shown). After 100 days of age, Tg mice with and without EGF and FGF2 treatment began to show motor symptoms, such as dragging and atrophy of the hindlimbs, but they remained alive until they were sacrificed 21 days after minipump placement. No significant differences were observed between the groups with respect to body weight at this time (Table I). However, the Tg mice had significantly reduced rotarod scores ($P < 0.01$) in the groups with and without EGF and FGF2 compared with both groups of non-Tg mice. The rotarod scores were not significantly different in the Tg groups with and without EGF and FGF2.

Histological Observations

Histological evaluation of the L4 segment revealed substantial motor neuron loss in the VH of Tg mice treated with vehicle (230.5 ± 91.0, $P < 0.01$) compared with non-Tg mice treated with vehicle (561.4 ± 107.0) and in the VH of Tg mice treated with EGF and FGF2 (266.0 ± 80.4, $P < 0.01$) compared with non-Tg mice treated with EGF and FGF2 (563.5 ± 111.1; Fig. 2). However, treatment with EGF and FGF2 (266.0 ± 80.4) did not ameliorate motor neuron loss in Tg mice compared with Tg mice treated with vehicle (230.5 ± 91.0). Immunostaining for ChAT supported these results (data not shown).

Changes in BrdU-Labeled Cell

Among the two vehicle-treated groups, the total number of BrdU-labeled cells increased 2.0-fold in the lumbar spinal cords of Tg mice compared with the non-Tg mice at 21 days after minipump placement (Fig. 3, Table II). Upon regional analysis, most BrdU-labeled cells were found to be located in the WM, with some in the GM and CC (Fig. 3, Table II). This pattern was consistent in non-Tg and Tg mice. Upon closer analysis of the GM, the numbers of BrdU-labeled cells were found to be increased more in the VH than in the DH in Tg mice, although the number of BrdU-labeled cells was greater in the DH than the VH in non-Tg mice (Fig. 3, Table II).

With EGF and FGF2 treatment, the total number of BrdU-labeled cells in the lumbar spinal cord of both non-Tg and Tg mice increased 2.3- and 2.1-fold compared with the vehicle groups, respectively, and the total number of BrdU-labeled cells in the Tg mice was 1.9-fold that of the non-Tg group (Fig. 3, Table II). Upon regional analysis, the numbers of BrdU-labeled cells were found to be increased in all regions (WM, GM, and CC) in mice treated with EGF and FGF2 compared with vehicle treatment in both non-Tg and Tg mice (Fig. 3, Table II). Although most BrdU-labeled cells were located in the WM, with some in the GM and CC, the increase in the number of BrdU-labeled cells in the WM (1.0%) was smaller than that in the GM (1.2%) and CC (1.9%) in Tg mice treated with EGF and FGF2. Upon closer analysis of the GM, the number of BrdU-labeled cells increased more in both the VH and the DH relative to numbers in vehicle-treated mice in both non-Tg and Tg groups, and the number of BrdU-labeled cells increased more in the VH (39.9 ± 14.0) than in the DH (30.9 ± 13.3, $P < 0.01$) in Tg mice, although the increase was greater in the DH in non-Tg mice (Fig. 3, Table II).

Double-Immunofluorescence Analysis

Double labelling with BrdU and nestin, PSA-NCAM, Iba1, NeuN, or GFAP showed that many BrdU-labeled cells expressed nestin and also (but to a lesser extent) Iba1, GFAP, and PSA-NCAM, but none expressed NeuN in the lumbar spinal cords of either non-Tg or Tg mice with or without EGF and FGF2 treatment (Fig. 3, Table II). With EGF and FGF2 treatment, the increases in the rates of BrdU + nestin, PSA-NCAM, Iba1, or GFAP double-labeled cells in Tg mice were 1.3, 1.6, 1.2, and 0.5, respectively, so the increase in the rate of BrdU + nestin and BrdU + PSA-NCAM double-labeled cells was greater than that of BrdU + GFAP. Upon regional analysis of the GM of Tg mice treated with EGF and FGF2, the number of BrdU + nestin double-labeled cells was

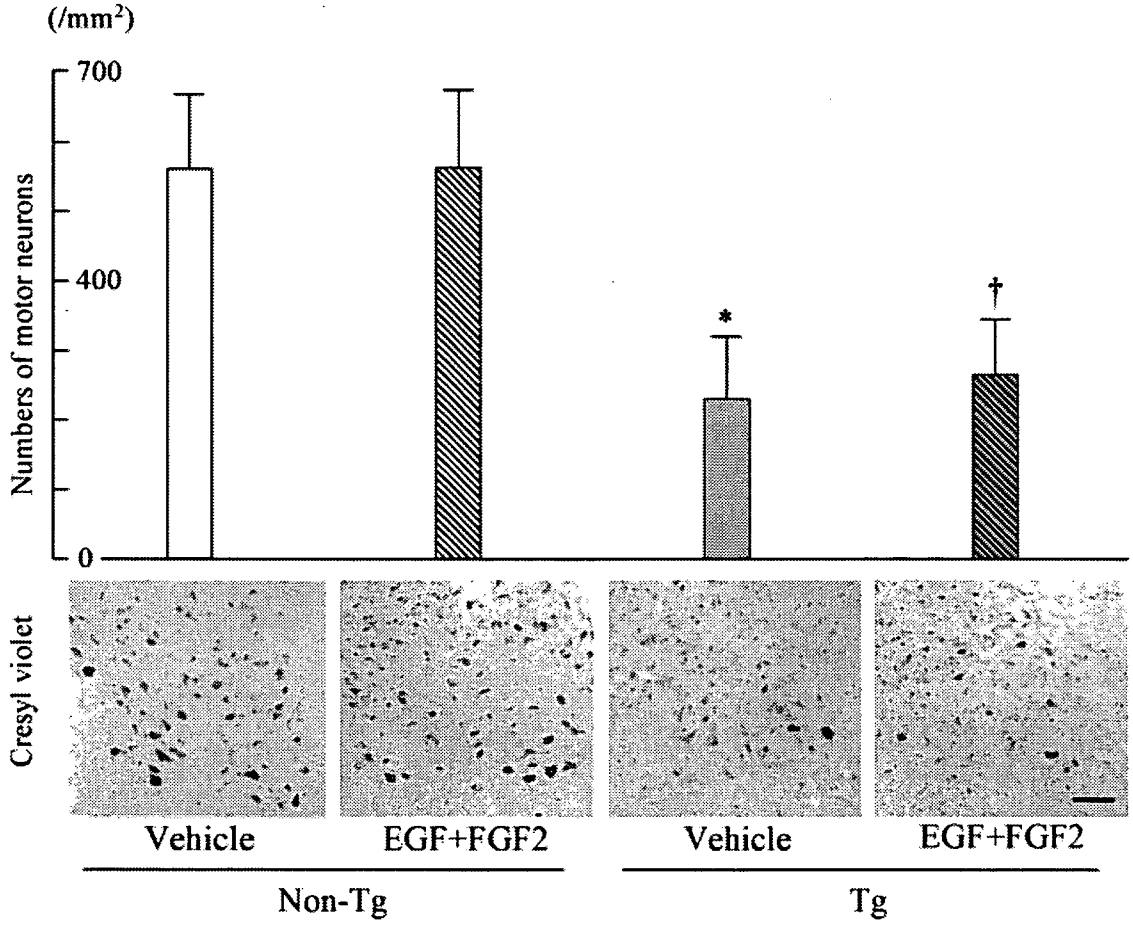

Fig. 2. Numbers (upper panel) and representative photomicrographs (lower panels) of motor neurons in the ventral horns (VH) of both non-Tg and Tg mice. Note the substantial motor neuron loss in Tg mice with or without EGF and FGF2 treatment compared with non-Tg mice (data are mean ± SD, $*P < 0.01$ vs. non-Tg mice treated with vehicle; $^{\dagger}P < 0.01$ vs. non-Tg mice treated with EGF and FGF2). Also note the similar numbers of motor neurons in Tg mice treated with vehicle and EGF and FGF2. Scale bar = 100 μm.

found to be larger than the number of BrdU + Iba1, BrdU + GFAP, and BrdU + PSA-NCAM double-labeled cells in the VH (Figs. 3, 4A,E,I,M, Table II) and in the DH (Figs. 3, 4B,F,J,N, Table II). Although the number of PSA-NCAM single-labeled cells and BrdU + PSA-NCAM double-labeled cells was smaller than the number of BrdU + nestin, BrdU + Iba1, or BrdU + GFAP double-labeled cells in the GM of both non-Tg and Tg mice, the increases in the rates of BrdU + PSA-NCAM double-labeled cells (3.2) were larger than those of BrdU + nestin (2.4), BrdU + Iba1 (1.2), or BrdU + GFAP (0.4) double-labeled cells in the GM of Tg mice with EGF and FGF2 treatment (Figs. 3, 4A,B,E,F,I,J,M,N, Table II). Although the number of nestin single-labeled cells increased less relative to Iba1 and GFAP in the GM, those in the WM increased more relative to Iba1 and GFAP in both non-Tg and Tg mice. Many BrdU-labeled cells expressed nestin and also (but to lesser extents) Iba1, GFAP, and PSA-NCAM in the WM of both non-Tg and Tg mice (Figs. 3, 4C,G,K,O, Table II). The number of nestin and PSA-NCAM single-labeled cells increased more relative to those labeled with Iba1 and GFAP in the CC of Tg mice, and the number of BrdU + nestin and BrdU + PSA-NCAM double-labeled cells was greater than the number of BrdU + Iba1 and BrdU + GFAP double-labeled cells (Figs. 3, 4D,H,L,P, Table II). Upon closer analysis of the GM, the number of BrdU + nestin double-labeled cells was found to be larger than the number of BrdU + Iba1, BrdU + GFAP, and BrdU + PSA-NCAM double-labeled cells only in the VH of Tg mice treated with EGF and FGF2, although the number of BrdU + Iba1 double-labeled cells was larger than the number of BrdU + nestin, BrdU + GFAP, and BrdU + PSA-NCAM double-labeled cells in both the VH and the DH of Tg mice treated with vehicle and non-Tg mice treated with vehicle and EGF and FGF2. (Figs. 3, 4A,B,E,F,I,J,M,N, Table II).

The total number of BrdU + nestin double-labeled cells in the vehicle-treated groups increased 3.7-fold in

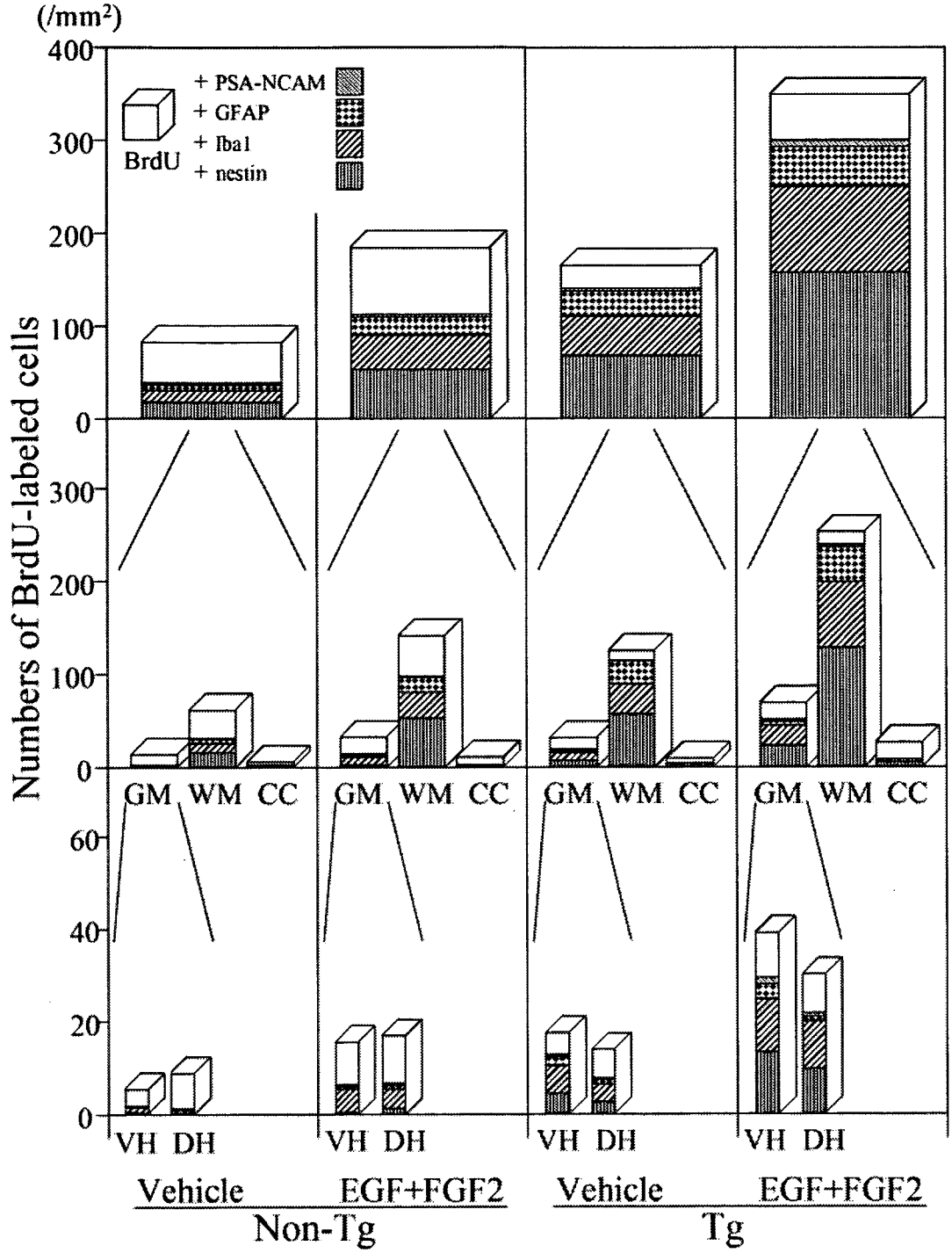

Fig. 3. Total numbers of BrdU-labeled cells and double-labeled cells with nestin, Iba1, GFAP, or PSA-NCAM in the lumbar spinal cords of all groups (top panels). Regional differences between the gray matter (GM), white matter (WM), and the ependyma of the central canal (CC; middle panels), and closer analysis of the VH and dorsal horns (DH) in the GM (bottom panels). Note that the total number of BrdU-labeled and BrdU + nestin double-labeled cells greatly increased in Tg mice treated with EGF and FGF2 (top panels). Upon regional analysis, the majority of BrdU-labeled and BrdU + nestin double-labeled cells were found to be located in the WM, with some in the GM and CC (middle panels). Closer analysis of the GM in vehicle-treated Tg mice revealed that the number of BrdU-labeled and BrdU + nestin double-labeled cells increased more in the VH than in the DH, which was greatly enhanced by treatment with EGF and FGF2 (bottom panels). See Results for details.

Tg mice (68.6 ± 49.7) compared with non-Tg mice (18.6 ± 14.2, $P < 0.01$; Fig. 3, Table II). Furthermore, the proportion of the total BrdU-labeled cells represented by the total BrdU + nestin double-labeled cells was larger in Tg mice (40.9%) than that in non-Tg mice (22.3%). Upon regional analysis, most BrdU + nestin double-labeled cells were found to be located in the WM, with some in the GM and CC in both non-Tg and Tg mice (Fig. 3, Table II). The proportion of BrdU-labeled cells represented by BrdU + nestin double-labeled cells was larger in the WM (non-Tg 27.1%; Tg 46.4%) than the GM in both non-Tg and Tg mice (non-Tg 3.5%; Tg 21.9%). The number of BrdU + nestin double-labeled cells and the proportion of those in the WM and GM of Tg mice (WM 46.4%; GM 21.9%) was larger than in non-Tg mice (WM 27.1%; GM

TABLE II. Numbers of BrdU-Labeled Cells and Double-Labeled Cells With Nestin, Ibal, GFAP, or PSA-NCAM in the Lumbar Spinal Cords†

Numbers of BrdU-labeled cells (/mm^2)	Non-Tg		Tg	
	Vehicle	EGF + FGF2	Vehicle	EGF + FGF2
BrdU				
Total	83.3 ± 31.8	187.9 ± 62.8*	167.7 ± 65.7*	354.6 ± 83.8**,***
Gray matter	14.4 ± 10.1	33.2 ± 16.5*	32.0 ± 15.8*	70.8 ± 25.0**,***
Ventral hom	5.5 ± 4.4	15.9 ± 9.2	17.7 ± 7.3****	39.9 ± 14.0*****
Dorsal hom	9.0 ± 6.5	17.4 ± 8.7	14.2 ± 9.3	30.9 ± 13.3
White matter	62.1 ± 27.3	143.0 ± 56.7*	126.2 ± 52.7*	256.7 ± 74.5**,***
Central canal	6.8 ± 5.9	11.7 ± 11.8	9.5 ± 7.4	27.2 ± 25.5**,***
BrdU + nestin				
Total	18.6 ± 14.2	54.7 ± 33.2	68.6 ± 49.7*	159.3 ± 89.2**
Gray matter	0.5 ± 0.8	1.3 ± 1.7	7.0 ± 6.7*	23.6 ± 15.2**
Ventral hom	0.1 ± 0.4	0.2 ± 0.5	4.4 ± 3.9	13.6 ± 9.9
Dorsal hom	0.3 ± 0.8	1.2 ± 1.4	2.5 ± 3.1	10.0 ± 6.1
White matter	16.8 ± 14.0	53.1 ± 32.9	58.5 ± 40.8*	130.4 ± 76.2**
Central canal	1.2 ± 3.1	0.2 ± 0.7	3.0 ± 5.5	5.3 ± 6.3
BrdU + Ibal				
Total	13.2 ± 14.1	38.2 ± 21.2	43.8 ± 26.2*	94.9 ± 55.3**
Gray matter	1.9 ± 2.4	9.5 ± 12.9	9.9 ± 10.8*	22.1 ± 19.0*
Ventral hom	1.2 ± 2.0	5.2 ± 8.0	6.1 ± 4.9	11.7 ± 10.1
Dorsal hom	0.6 ± 1.1	4.2 ± 4.9	3.9 ± 6.5	10.5 ± 11.3
White matter	11.3 ± 12.2	28.7 ± 16.0	33.8 ± 18.4*	72.7 ± 42.9**
Central canal	0.0 ± 0.0	0.0 ± 0.0	0.0 ± 0.0	0.0 ± 0.0
BrdU + GFAP				
Total	6.0 ± 5.5	19.0 ± 15.1	28.9 ± 17.8*	43.7 ± 17.9**
Gray matter	0.4 ± 0.6	1.5 ± 1.4	3.0 ± 3.4*	4.3 ± 5.6
Ventral hom	0.2 ± 0.5	0.6 ± 1.0	1.9 ± 2.8	3.4 ± 4.4
Dorsal hom	0.1 ± 0.5	0.9 ± 1.0	1.1 ± 1.4	1.0 ± 1.4
White matter	5.6 ± 5.6	17.1 ± 14.2	25.6 ± 15.8*	38.4 ± 14.8**
Central canal	0.0 ± 0.0	0.4 ± 1.4	0.3 ± 1.3	0.9 ± 2.7
BrdU + PSA-NCAM				
Total	2.1 ± 3.0	3.3 ± 2.7	3.1 ± 3.3	8.1 ± 7.1
Gray matter	0.0 ± 0.0	1.0 ± 1.5	0.6 ± 1.0	2.5 ± 3.7
Ventral hom	0.0 ± 0.0	0.4 ± 1.0	0.4 ± 0.9	1.6 ± 2.7
Dorsal hom	0.0 ± 0.0	0.6 ± 1.4	0.2 ± 0.6	0.8 ± 1.7
White matter	0.5 ± 0.5	0.7 ± 0.8	1.1 ± 1.3	2.9 ± 2.2**
Central canal	1.6 ± 2.6	1.6 ± 2.6	1.4 ± 2.4	2.7 ± 6.6

†After placement of the minipump, 50 mg/kg BrdU was intraperitoneally injected every 6 hr (four times per day) for 7 days, a total of 28 injections. At 121 days of age (21 days after minipump placement), total number; regional differences between the gray matter, white matter, and the ependyma of the central canal; and closer analysis of the ventral homs and dorsal homs in the gray matter of BrdU-labeled cells and double-labeled cells with nestin, Ibal, GFAP, or PSA-NCAM in the lumbar spinal cords (/mm^2) were evaluated. Data are presented as mean ± SD.

*$P < 0.01$ compared with non-Tg mice with vehicle.

**$P < 0.01$ compared with non-Tg mice with EGF and FGF2.

***$P < 0.01$ compared with Tg mice with vehicle.

****$P < 0.05$ compared with the posterior sides of Tg mice with vehicle.

*****$P < 0.01$ compared with the posterior sides of Tg mice with EGF and FGF2.

3.5%). Upon closer analysis of the GM in Tg mice, the number of BrdU + nestin double-labeled cells was found to be increased more in the VH (4.4 ± 3.9) than in the DH (2.5 ± 3.1; Fig. 3, Table II). The proportion of BrdU + nestin double-labeled cells in the VH (25.8%) was larger than that in the DH (17.6%).

With EGF and FGF2 treatment, the total number of BrdU + nestin double-labeled cells in both non-Tg and Tg mice (54.7 ± 33.2, 159.3 ± 89.2) increased 2.9- and 2.3-fold, respectively, compared with vehicle-treated mice (18.6 ± 14.2, 68.6 ± 49.7), and the total number of BrdU + nestin double-labeled cells in Tg mice (159.3 ± 89.2) was 2.9-fold that in non-Tg mice (54.7 ± 33.2, $P < 0.01$; Fig. 3, Table II). The proportion of total BrdU-labeled cells represented by total BrdU + nestin double-labeled cells was larger (non-Tg 29.1%; Tg 44.9%) in the EGF and FGF2 treated groups than in the vehicle-treated groups (non-Tg; 22.3%, Tg; 40.9%). Upon regional analysis, the number of BrdU + nestin double-labeled cells was found to be increased in the WM and GM relative to the vehicle

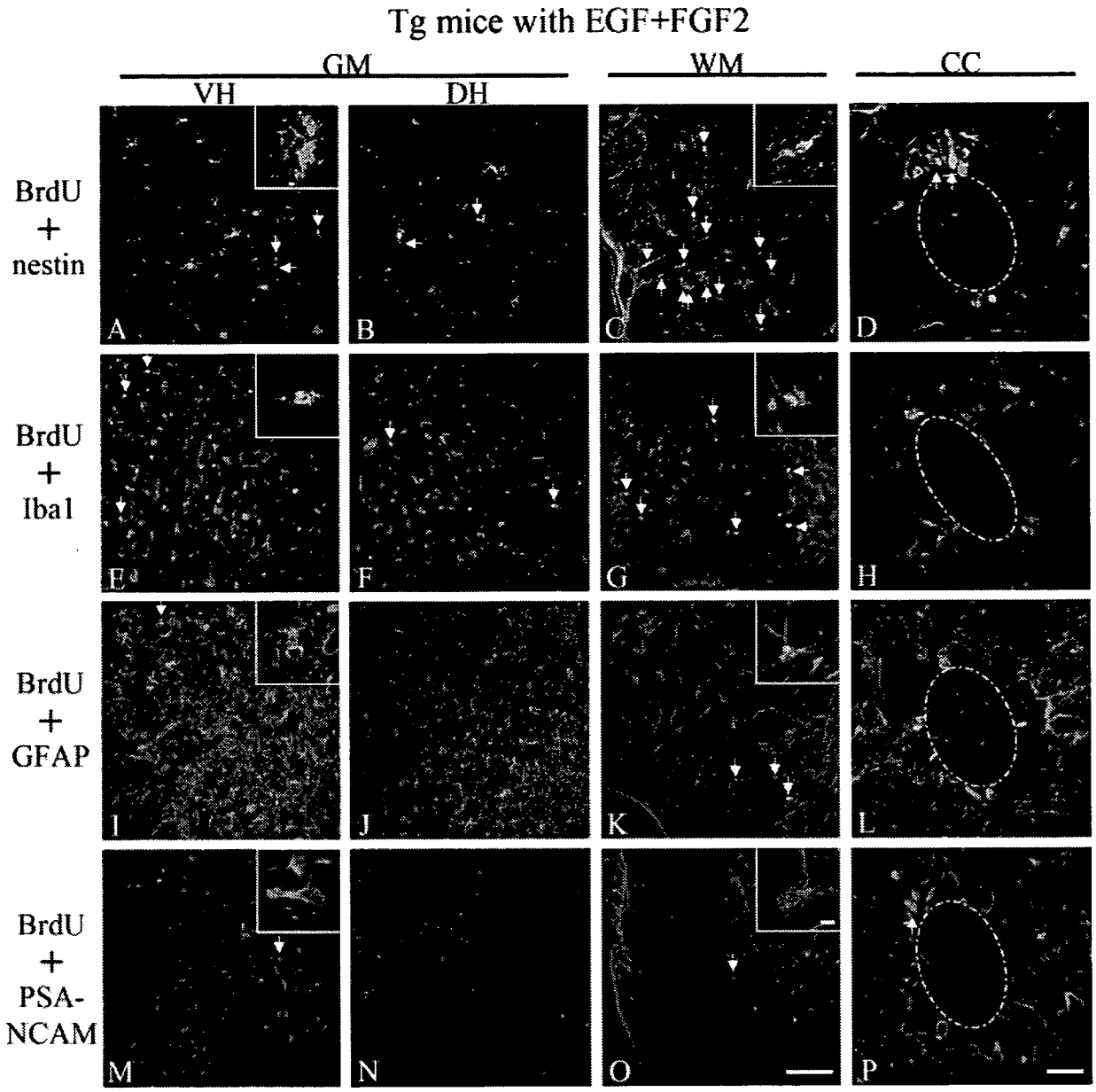

Fig. 4. Double-immunofluorescence analysis for BrdU (green) and nestin, Iba1, GFAP, PSA-NCAM (red) in Tg mice treated with EGF and FGF2. Many BrdU-labeled cells expressed nestin and also (to a lesser extent) Iba1, GFAP, and PSA-NCAM in the VH (**A,E,I,M,** arrows), DH (**B,F,** arrows; **J,N**), WM (**C,G,K,O,** arrows) and CC (**D,P,** arrows; **H,L**). Closer analysis of the GM showed that BrdU + nestin, Iba1, GFAP, and PSA-NCAM double-labeled cells increased more in the VH (A,E,I,M, arrows) than in the DH (B,F, arrows; J,N). The dashed circles in D,H,L,P indicate the central canal. Scale bars = 100 μm in O (applies to A–C,E–G,I–K,M–O); 10 μm in insets; 20 μm in P (applies to D,H,L,P).

in both non-Tg and Tg mice treated with EGF and FGF2, and that most nestin single-labeled and BrdU + nestin double-labeled cells were located in the WM, with some in the GM and CC (Figs. 3, 4A–D, Table II). However, the increase in the rate of BrdU + nestin double-labeled cells in the GM (2.4%) was larger than that in the WM (1.2%) and CC (0.8%) in Tg mice treated with EGF and FGF2. The proportion of BrdU-labeled cells in the WM and GM represented by the number of double-labeled cells in mice treated with EGF and FGF2 (non-Tg WM 37.1%; GM 3.9%; Tg WM 50.8%; GM 33.3%) was larger than that in the vehicle-treated mice (non-Tg WM 27.1%; GM 3.5%; Tg WM 46.4%; GM 21.9%). The same proportion in the WM and GM of Tg mice treated with EGF and FGF2 (WM; 50.8%, GM; 33.3%) was much larger than that in non-Tg mice treated with EGF and FGF2 (WM; 37.1%, GM; 3.9%). Upon closer analysis of the GM in both non-Tg and Tg mice treated with EGF and FGF2, the number

of BrdU + nestin double-labeled cells increased in both the VH and the DH compared with the vehicle-treated mice, and the number of nestin single-labeled and BrdU + nestin double-labeled cells increased more in the VH than in the DH in Tg mice (Figs. 3, 4A,B, Table II). In Tg mice, the proportion of BrdU-labeled cells represented by BrdU + nestin double-labeled cells in both VH and DH (VH 34.1%; DH 33.3%) was larger than that in vehicle-treated mice (VH 25.8%; DH 17.6%), and the number of those in the VH increased 3.1-fold compared with vehicle-treated mice.

The total number of BrdU + Iba1 double-labeled cells in the vehicle-treated groups increased 3.3-fold in Tg mice (43.8 ± 26.2) compared with the non-Tg mice (13.2 ± 14.1, $P < 0.01$; Fig. 3, Table II). Upon regional analysis, most BrdU + Iba1 double-labeled cells were found to be located in the WM, with some in the GM in both non-Tg and Tg mice (Fig. 3, Table II). Although the proportion of BrdU-labeled cells represented by BrdU + Iba1 double-labeled cells was larger in the WM (18.2%) than in the GM (13.2%) in non-Tg mice, the proportion was smaller in the WM (26.8%) than in the GM (30.9%) in Tg mice. Upon closer analysis of the GM in both non-Tg and Tg mice, the number of BrdU + Iba1 double-labeled cells were found to be increased more in the VH than in the DH (Fig. 3, Table II). With EGF and FGF2 treatment, the total number of BrdU + Iba1 double-labeled cells in both non-Tg and Tg mice increased 2.9- and 2.2-fold compared with that vehicle-treated mice (Fig. 3, Table II), respectively. Upon regional analysis, the numbers of BrdU + Iba1 double-labeled cells were found to be increased in the WM and GM in mice treated with EGF and FGF2 compared with vehicle-treated mice in both the non-Tg and the Tg groups, and most BrdU + Iba1 double-labeled cells were located in the WM, with some in the GM in both non-Tg and Tg mice, although the Iba1 single-labeled cells were located more in the GM, with some in the WM and CC in Tg mice (Figs. 3, 4E–H, Table II). Upon closer analysis of the GM in both non-Tg and Tg mice, the numbers of BrdU + Iba1 double-labeled cells were found to be increased in mice treated with EGF and FGF2 in both the VH and the DH compared with vehicle-treated mice, and the numbers of Iba1 single-labeled and BrdU + Iba1 double-labeled cells increased more in the VH than in the DH in Tg mice (Figs. 3, 4E,F, Table II).

The total number of BrdU + GFAP double-labeled cells in the vehicle-treated groups increased 4.8-fold in Tg mice (28.9 ± 17.8) compared with the non-Tg mice (6.0 ± 5.5, $P < 0.01$; Fig. 3, Table II). Upon regional analysis, most BrdU + GFAP double-labeled cells were found to be located in the WM, with some in the GM and CC in both non-Tg and Tg mice (Fig. 3, Table II). Upon closer analysis of the GM in both non-Tg and Tg mice, the number of BrdU + GFAP double-labeled cells was found to be increased more in the VH than in the DH (Fig. 3, Table II). With EGF and FGF2 treatment, the total number of BrdU + GFAP double-labeled cells in both non-Tg and Tg mice increased 3.2- and 1.5-fold compared with the vehicle-treated groups (Fig. 3, Table II), respectively. Upon regional analysis, the numbers of BrdU + GFAP double-labeled cells were found to be increased in the WM, GM, and CC in mice treated with EGF and FGF2 compared with the vehicle-treated groups for both non-Tg and Tg mice, and the majority of BrdU + GFAP double-labeled cells were located in the WM, with some in the GM and the CC in both non-Tg and Tg mice, although GFAP single-labeled cells were located mostly in the GM, with some in the WM and CC of Tg mice (Figs. 3, 4I–L, Table II). Upon closer analysis of the GM in Tg mice, the numbers of BrdU + GFAP double-labeled cells were found to be increased in the VH in mice treated with EGF and FGF2 compared with vehicle-treated mice, and the numbers of GFAP single-labeled and BrdU + GFAP double-labeled cells increased more in the VH than in the DH in Tg mice (Figs. 3, 4I,J, Table II).

The total number of BrdU + PSA-NCAM double-labeled cells in the vehicle-treated groups increased 1.5-fold in Tg mice (3.1 ± 3.3) compared with the non-Tg mice (2.1 ± 3.0; Fig. 3, Table II). Upon regional analysis, most BrdU + PSA-NCAM double-labeled cells were found to be located in the CC in both non-Tg and Tg mice (Figs. 3, 4E–H, Table II). Upon closer analysis of the GM in Tg mice, the numbers of BrdU + PSA-NCAM double-labeled cells were found to be increased more in the VH than in the DH (Fig. 3, Table II). With EGF and FGF2 treatment, the total number of BrdU + PSA-NCAM double-labeled cells in both non-Tg and Tg mice increased 2.5- and 1.5-fold compared with the vehicle-treated groups (Fig. 3, Table II), respectively. Upon regional analysis, the numbers of BrdU + PSA-NCAM double-labeled cells were found to be increased in the WM, GM, and CC in mice treated with EGF and FGF2 compared with the vehicle-treated groups for both non-Tg and Tg mice. The BrdU + PSA-NCAM double-labeled cells were located in the GM, WM, and CC equally in Tg mice, but the increase in the rate of BrdU + PSA-NCAM double-labeled cells in GM (3.2) was larger than that of WM (1.6) and CC (0.9), and PSA-NCAM single-labeled cells were located mostly in the GM and CC of Tg mice (Figs. 3, 4M–P, Table II). Upon closer analysis of the GM in Tg mice, the numbers of BrdU + PSA-NCAM double-labeled cells were found to be increased in both VH and DH in mice treated with EGF and FGF2 compared with vehicle-treated mice, and the number of PSA-NCAM single-labeled and BrdU + PSA-NCAM double-labeled cells increased more in the VH than in the DH in Tg mice (Figs. 3, 4M,N, Table II).

Triple-Immunofluorescence Analysis

Upon regional analysis, many nestin single-labeled cells expressed GFAP in the GM and WM of both non-Tg and Tg mice with or without EGF and FGF2 (Fig. 5A,B), but nestin single-labeled cells rarely expressed

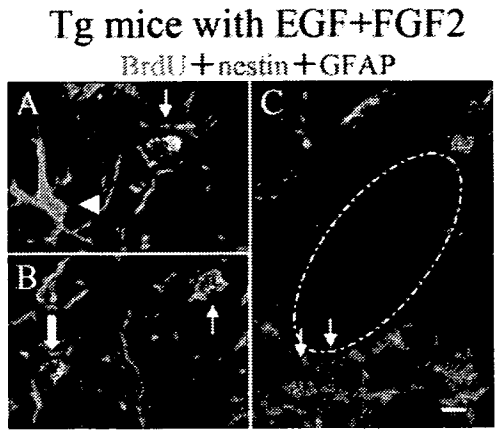

Fig. 5. Triple-immunofluorescence analysis for BrdU (green), nestin (red), and GFAP (blue) in Tg mice treated with EGF and FGF2. Many of the BrdU + nestin double-labeled cells did not express GFAP in the VH of GM (**A**; small arrow), WM (**B**; small arrow) and CC (**C**; small arrows), but many nestin single-labeled cells expressed GFAP in the GM (A; arrowhead) and WM, and some of the BrdU + nestin double-labeled cells expressed GFAP in the GM and WM (B; large arrow). The dashed circle indicates the central canal. Scale bar = 10 μm.

GFAP in the CC (Fig. 5C). The majority of BrdU + nestin double-labeled cells did not express GFAP in the CC of either non-Tg or Tg mice with or without EGF and FGF2 (Fig. 5C). In the GM and WM, many of the BrdU + nestin double-labeled cells did not express GFAP, but some of them expressed GFAP (Fig. 5A,B). In the case of BrdU + GFAP double-labeled cells, most of them expressed nestin in the GM, WM, and CC.

DISCUSSION

In the present study, we first observed that the number of BrdU + nestin double-labeled cells increased 3.7-fold in the spinal cords of Tg mice even without EGF and FGF2 treatment compared with non-Tg mice (Fig. 3, Table II). Treatment with EGF and FGF2 greatly increased the number of BrdU + nestin double-labeled cells in the spinal cords of both non-Tg and Tg mice (Fig. 3, Table II). With closer analysis of the GM of vehicle-treated groups, the number of BrdU + nestin double-labeled cells increased more in the VH than in the DH in Tg mice (Fig. 3, Table II), which was greatly enhanced by treatment with EGF and FGF2.

Among the vehicle-treated groups, the total number of BrdU-labeled cells increased 2.0-fold in the lumbar spinal cords of Tg mice compared with non-Tg mice at 21 days after minipump placement (Fig. 3, Table II), indicating that cell proliferation becomes active in Tg mice that have ALS. Double-labelling with BrdU + nestin, Iba1, GFAP, PSA-NCAM, or NeuN showed that many BrdU-labeled cells expressed nestin, and also Iba1, GFAP, and PSA-NCAM to a lesser extent, in both non-Tg and Tg mice but did not express NeuN. Although expression of nestin in the CNS is generally considered the marker of neural precursor cells (Reynolds and Weiss, 1992; Weiss et al., 1996; Gritti et al., 1996; Namiki and Tator, 1999; Schwartz et al., 2003; Chi et al., 2006), recent reports indicate that certain populations of adult neural precursor cells express GFAP (Doetsch et al., 1999; Rietze et al., 2001; Barres, 2003; Imura et al., 2003), and reactive astrocytes or immature astrocytes also express nestin in the injured spinal cord (Frisen et al., 1995; Lang et al., 2004). In the triple-immunofluorescence studies using BrdU, nestin, and GFAP, many BrdU + nestin-labeled cells did not express GFAP in the GM, WM, or CC, but some of them expressed GFAP in the GM and WM. The GFAP-negative BrdU + nestin double-labeled cells indicate the presence of real neural precurosor cells. However, BrdU + nestin + GFAP triple-labeled cells indicate the presence of astrocytogenesis or reactive astrocytosis, but some of them might be neural precursor cells too. As a result, we consider that most of the BrdU + nestin double-labeled cells are proliferating neural precursor cells. As previously determined for normal and pathological spinal cord (Horner et al., 2000; Strong et al., 2004; Zai and Wrathall, 2005; Chi et al., 2006), neural precursor cells proliferated more in Tg mice than in non-Tg mice and also proliferated more than microglial cells in both non-Tg and Tg mice. In an ischemic insult to the brain, the expression of the endogenous growth factors, such as EGF and FGF2, was significantly elevated (Naylor et al., 2005). In the spinal cords of mice with ALS, endogenous growth factors such as EGF and FGF2 might increase and neural precursor cells proliferate as a result.

Both EGF and FGF2 have neuroprotective effects against ischemic brain and spinal cord injury (Bethel et al., 1997; Kiprianova et al., 1999; Kojima and Tator, 2002), and they also have mitogenic effects on neural precursor cells in adult mouse or rat brain and spinal cord (Weiss et al., 1996; Kojima and Tator, 2002; Nakatomi et al., 2002; Martens et al., 2002). Although combination treatment with EGF and FGF2 may protect dying motor neurons in the spinal cords of mice with ALS, the present results indicate no such protective effect (Fig. 2, Table I). Neural regeneration can be divided into three steps: proliferation, migration, and differentiation (Gage, 2000; Iwai et al., 2002). Thus, we injected both EGF and FGF2 over only 7 days to stimulate neural precursor cell proliferation and sacrificed the mice 21 days after minipump placement to observe the migration and differentiation of the newly produced neural precursor cells during days 14–21. This treatment increased the numbers of BrdU + nestin, BrdU + PSA-NCAM, and BrdU + GFAP double-labeled cells relative to those in vehicle-treated mice, and the increase in the rate of BrdU + PSA-NCAM double-labeled cells was larger than that for BrdU + GFAP in GM of Tg mice (Fig. 3, Table II). Because the expression of PSA-NCAM in the CNS is generally considered a marker of neuronal precursor cells (Seki and Arai, 1993; Bonfanti and Theodosis, 1994; Rousselot et al., 1995; Doetsch and Alvarez-Buylla, 1996; Lois et al., 1996), we consider that the BrdU + PSA-NCAM double-labeled cells could

be proliferating neuronal precursor cells in the GM and CC. These results indicate that treatment with EGF and FGF2 potentiates the proliferation of neural precursor cells and their differentiation into neuronal precursor cells instead of astrocytes in GM of Tg mice.

A previous study showed that the majority of BrdU-labeled cells were located in the WM even at 1 hr after intraperitoneal BrdU injection in the normal spinal cord (Horner et al., 2000). Because neural precursor cells in the spinal cord reportedly reside close to the CC (Johansson et al., 1999; Martens et al., 2002), cells would be able to migrate from the CC to the WM rapidly. Nestin-labeled cells proliferate in the CC immediately after injury or after EGF and FGF2 treatment, and then the number in the CC is diminished because of migration to the WM and GM (Namiki and Tator, 1999; Kojima and Tator, 2002); astrocytes and oligodendrocytes increase slightly in the WM after injury or after EGF and FGF2 treatment (Martens et al., 2002; Zai and Wrathall, 2005). In the present study, most BrdU + nestin double-labeled cells were located in the WM, with some in the GM and CC, in all groups (Fig. 3, Table II). This suggests that most neural precursor cells that proliferated in the CC during BrdU labelling rapidly migrated to the WM, but few differentiated into astrocytes in the WM during the subsequent days 8–21. Although we did not extensively study oligodendrocytes, it appears that neural precursor cells seldom differentiated into oligodendrocytes in the WM.

Closer analysis of the GM showed that Tg itself increased the number of BrdU + nestin and BrdU + PSA-NCAM double-labeled cells, especially in the VH rather than the DH, which was greatly enhanced by treatment with EGF and FGF2 (Fig. 3, Table II). These results indicate that the migration of neural precursor cells to the VH with differentiation into neuronal precursor cells in VH is stimulated by motor neuron death associated with the SOD1 mutation and that EGF and FGF2 treatment enhances this migration of neural precursor cells to the GM and differentiation into neuronal precursor cells in the GM. In fact, treatment with EGF and FGF2 not only caused the proliferation of neural precursor cells but also potentiated their migration to the hippocampus and differentitaion into neuronal precursor cells and neurons after transient cerebral ischemia (Nakatomi et al., 2002).

The number of BrdU + nestin double-labeled cells was greater than the number of BrdU + GFAP double-labeled cells in the VH (Figs. 3, 4A,E,I, Table II) and DH (Figs. 3, 4B,F,J, Table II) of Tg mice, although the number of nestin single-labeled cells increased less than the number of GFAP single-labeled cells in the GM of Tg mice. Because most neural precursor cells remain immature rather than differentiating into astrocytes at 14–21 days after proliferation (Horner et al., 2000; Zai and Wrathall, 2005) and astrocytes start to increase in number in the GM, especially in the VH, during the presymptomatic stages of ALS (Hall et al., 1998; Yoshihara et al., 2002), most astrocytes observed at 21 days after minipump placement (Fig. 4I–L) were the cells that differentiated during the presymptomatic stages from neural precursor cells. Only small numbers of neural precursor cells differentiate into astrocytes during the symptomatic stages of ALS (Figs. 3, 4I–L, Table II), or they might have differentiated into astrocytes after 14 days (Kojima and Tator, 2002). Microglial cells are derived mainly from monocytes in pathological conditions (Kreutzberg, 1996), and they proliferate in the spinal cord during symptomatic ALS (Hall et al., 1998; Azari et al., 2005). Although some BrdU + Iba1 double-labeled cells might be BrdU-containing microglias resulting from phagocytosis, most of them will be labeled because of microglial proliferation. In the present study, microglial cells proliferated both in the WM and in the GM of Tg mice even with vehicle treatment (Fig. 3, Table II), and proliferation was enhanced both in non-Tg and in Tg mice with EGF and FGF2 treatment (Figs. 3, 4E–H, Table II).

In previous studies, neurogenesis was found in the subventricular zone of the lateral ventricle (Altman, 1969; Doetsch et al., 1997; Kornack and Rakic, 2001; Pencea et al., 2001) and the dentate gyrus of the hippocampus (Altman and Das, 1965; Kaplan and Hinds, 1977; Bayer et al., 1982; Cameron and McKay, 2001). Although extensive proliferation of intrinsic neural precursor cell activation and neurogenesis have been observed in the hippocampus after transient global ischemia with EGF and FGF2 treatment (Nakatomi et al., 2002), such activation has not been observed in pathological spinal cord even with EGF and FGF2 treatment (Gritti et al., 1996; Horner et al., 2000; Martens et al., 2002; Kojima and Tator, 2002; Mothe and Tator, 2005). Furthermore, in the present study, BrdU + NeuN double-labeled cells were not observed in Tg mice even with EGF and FGF2 treatment, although BrdU + PSA-NCAM double-labeled cells slightly increased in VH of Tg mice. However, the present study revealed extensive proliferation and migration of neural precursor cells to the VH, where they differentiate into neuronal precurosor cells with EGF and FGF2 treatment. Thus, the next step will be to induce the neural precursor cells to differentiate into motor neurons where they are dying because of ALS.

ACKNOWLEDGMENTS

This work was partially supported by Grants-in-Aid for Scientific Research (B) 15390273 and (Hoga) 15659338 and the National Project on Protein Structural and Functional Analyses from the Ministry of Education, Science, Culture and Sports of Japan and by grants from the Ministry of Health and Welfare of Japan (to Y. Itoyama, I. Kimura, and S. Kuzuhara).

REFERENCES

Abe K, Morita S, Kikuchi T, Itoyama Y. 1997. Protective effect of a novel free radical scavenger, OPC-14117, on Wobbler mouse motor neuron disease. J Neurosci Res 48:63–70.